J. Fluid Mech. (2006), *vol.* 564, *pp.* 197–226.
doi:10.1017/S0022112006001510 Printed in the United Kingdom

Lagrangian mixing in decaying stably stratified turbulence

By SUBHAS K. VENAYAGAMOORTHY[1,2] AND DEREK D. STRETCH[1]

[1]School of Civil Engineering, University of KwaZulu-Natal, Durban, 4041, South Africa
[2]Environmental Fluid Mechanics Lab, Stanford University, Stanford, CA 94305-4020, USA

(Received 21 April 2005 and in revised form 7 March 2006)

Direct numerical simulations are used to study mixing and dispersion in decaying stably stratified turbulence from a Lagrangian perspective. The change in density of fluid particles owing to small-scale mixing is extracted from the simulations to provide insight into the mixing process. These changes are driven by temporally and spatially intermittent events that are strongly suppressed as the stratification increases and overturning motions disappear. This occurs for times $Nt > 2\pi$, i.e. after one buoyancy period, where N is the buoyancy frequency. The role of small-scale mixing processes in the density (or buoyancy) flux is analysed. After an initial transient, we find that diapycnal displacements due to mixing dominate the dispersion of fluid particles, even in weak stratification. The relationship between the diapycnal diffusivity and vertical dispersion coefficients is found to be strongly dependent on stratification. Models for the mixing following fluid particles are investigated. The time scale for the density changes due to small-scale mixing is shown to be approximately independent of N and instead remains linked to the energy decay time scale which is relatively insensitive to stratification. There are large changes in the structure of these flows as they evolve under the influence of buoyancy forces. We investigate these changes and their relationship to mixing. We find that strong mixing events are closely linked to the presence of overturning regions in the flow, and that they occur close to (but not within) these regions. The results reported here have implications for the development of improved models of diffusion in stably stratified turbulence.

1. Introduction

Most geophysical flows, such as in the oceans, atmosphere, lakes, or estuaries, are influenced by the presence of stable density stratification. Turbulent mixing in strongly stable flows often occurs during transient episodic events (e.g. due to the local breakdown of internal waves or from local shear instabilities) where there is no sustained source of energy. In these cases, the turbulence will subsequently decay and dissipate its initial energy. However, the mixing that takes place in such events could contribute significantly to overall mass/momentum balances and therefore be important for the understanding and modelling of these systems. Reviews of the structure and mixing of stably stratified geophysical flows are given by Gregg (1987) and Riley & Lelong (2000).

The ability to predict mixing and dispersion in stably stratified geophysical flows has many practical applications. For example, the management of air quality in the atmospheric boundary layer requires accurate models for predicting how turbulence

disperses pollutants released by industrial activities. The current generation of atmospheric dispersion models perform relatively poorly in stably stratified conditions (Nappo & Johansson 1999) which indicates a need for further work to improve their parameterizations.

A Lagrangian perspective, focusing on the advection of fluid particles, is a natural approach for studying mixing and dispersion in turbulent flows and dates back to the seminal work of G. I. Taylor (1921). Yeung (2002) gives a detailed review of results obtained from Lagrangian investigations. Lagrangian stochastic models have become increasingly important in problems involving turbulent mixing and dispersion. They also have a key role in turbulence models based on probability density function or PDF methods, which are especially suited to applications involving reacting flows (Pope 1994, 2000).

Pearson, Puttock & Hunt (1983, hereinafter referred to as PPH) developed a Lagrangian model of fluid particle dispersion in homogeneous, stationary, stably stratified turbulence. The PPH model explicitly accounts for small-scale mixing between fluid particles. They predict that vertical dispersion σ_z can cease to grow at intermediate times, but this is sensitive to a parameter in the theory that quantifies the rate of small-scale mixing between fluid particles. For times $t > N^{-1}$, their prediction can be written as

$$\sigma_z = (w'/N)\left(\zeta_z^2 + 2\gamma^2 N t\right)^{1/2}, \tag{1.1}$$

where ζ_z is an order unity dimensionless parameter that depends on the pressure gradient spectrum, and γ is a mixing coefficient that determines the rate at which the density of fluid particles changes owing to small-scale mixing. Therefore, if $\gamma \ll 1$, the model predicts that $\sigma_z \simeq w'/N \simeq$ *constant* for intermediate times $1 < Nt \lesssim \gamma^{-2}$. For larger times, or for large γ, the model predicts $\sigma_z \sim t^{1/2}$ in agreement with the classical diffusion limit. Hunt (1982, 1985) estimated that in the atmospheric boundary layer, γ typically varies in the range $0.1 < \gamma < 0.4$ which allows for both types of σ_z behaviour.

The importance of this issue was first revealed by Csanady (1964). In unstratified turbulence, fluid particles can move vertically over unlimited distances. Therefore large-scale vertical dispersion is relatively insensitive to small-scale molecular mixing. However, in stably stratified turbulence, work must be done against buoyancy forces to move fluid particles in the vertical. Therefore, without small-scale mixing, the available energy constrains the particle motions to vertical distances of order w'/N about their equilibrium density level. However, molecular diffusion can alter the fluid particle densities, which in turn alters the equilibrium levels about which they oscillate.

PPH developed the ideas of Csanady further, and argued that the vertical flux of density in a turbulent flow can be attributed to two processes: the first is the vertical displacements of fluid particles by advection, while the second involves the exchange of density between fluid particles. In stably stratified flows, PPH suggested that the second process can become dominant because of the aforementioned constraint on the vertical displacements. If this is the case, then in contrast to unstratified turbulence, small-scale mixing plays a crucial role in diffusion for stably stratified turbulence. Other models of diffusion in stably stratified turbulence (e.g. Venkatram, Strimaitis & Dicristofaro 1984) do not account explicitly for small-scale mixing and are based on an extension of classical statistical diffusion theory.

There have been no definitive validation studies of the PPH theory for diffusion in stably stratified fluids. Although PPH reported some comparisons with field and laboratory data (e.g. Britter *et al.* 1983), these were limited by the lack of direct

measurements of fundamental Lagrangian quantities used in their theory, particularly concerning the role of small-scale mixing processes. A deeper understanding of these processes therefore seems important for the development of improved models.

As a first step towards meeting this objective, we have performed direct numerical simulations of diffusion in transient (decaying) homogeneous stably stratified flows. DNS studies of diffusion in stably stratified turbulence have been reported by Kimura & Herring (1996) and Kaneda & Ishida (2000); however, they focused only on particle displacement statistics. A novel aspect of the work described here is our focus on the issue of how the densities of fluid particles change owing to small-scale mixing.

The key questions that we address in this study are as follows.

(i) What is the role of small-scale mixing processes in changes to the density perturbations ρ' following fluid particles? Both advection within the background mean density gradient and mixing contribute to changing ρ'. In § 4.3.1, we investigate how their roles change as buoyancy effects increase.

(ii) What is the role of small-scale mixing in the density (or buoyancy) flux of these flows? As noted above, contributions to the flux come from both the displacement (or segregation) of fluid particles and the mixing between fluid particles. We investigate this issue in § 4.3.2 and discuss how the role of small-scale mixing changes as the stratification strengthens.

(iii) How should small-scale mixing effects be incorporated into models of mixing and dispersion in stably stratified turbulence? We consider this issue in § 4.3.3, starting with the mixing model introduced by PPH.

(iv) How is Lagrangian mixing related to broader features of the flow such as overturning motions and internal waves? We address this question by examining the evolution of the flow structure in § 4.4.

2. Theoretical background

2.1. *Governing equations*

The governing conservation equations for the velocity and density fields are taken to be the Navier–Stokes equations with the Boussinesq approximation.

$$\frac{\mathrm{D}\boldsymbol{u}}{\mathrm{D}t} = -\frac{1}{\rho_0}\nabla p + \frac{\rho'}{\rho_0}\boldsymbol{g} + \nu\nabla^2\boldsymbol{u}, \tag{2.1a}$$

$$\nabla \cdot \boldsymbol{u} = 0, \tag{2.1b}$$

$$\frac{\mathrm{D}\rho}{\mathrm{D}t} = \kappa\nabla^2\rho, \tag{2.1c}$$

where $\boldsymbol{u} = (u, v, w)$ is the velocity vector, p is the kinematic pressure, $\boldsymbol{g} = (0, 0, -g)$, ρ_0 is a (constant) reference density, and ρ' is the density fluctuation relative to the local mean value, $\rho = \overline{\rho} + \rho'$.

Consider the case of a transient (i.e. decaying), homogeneous, stably stratified turbulence. Since the flow is homogeneous, the background mean density gradient is constant, with a buoyancy frequency given by $N^2 = -(g/\rho_0)(\partial\overline{\rho}/\partial z)$. The energetics of this flow, derived in the usual way from (2.1), is described by

$$\mathrm{d}(KE)/\mathrm{d}t = -b - \epsilon_{KE}, \tag{2.2a}$$

$$\mathrm{d}(PE)/\mathrm{d}t = \ b - \epsilon_{PE}, \tag{2.2b}$$

$$\mathrm{d}(E)/\mathrm{d}t = -\epsilon, \tag{2.2c}$$

where $KE = (u^2 + v^2 + w^2)/2$ is the turbulent kinetic energy, $PE = -\frac{1}{2}(g/\rho_0)(\partial\overline{\rho}/\partial z)^{-1}\overline{\rho'^2}$ is the (available) turbulent potential energy, $E = KE + PE$ is the total energy, $b = (g/\rho_0)\overline{\rho' w}$ is the buoyancy flux, and ϵ_{KE}, ϵ_{PE}, $\epsilon = (\epsilon_{KE} + \epsilon_{PE})$ are the dissipation rates of KE, PE and E, respectively. In this study, we focused on the case where the initial potential energy is zero.

2.2. *Lagrangian mixing*

The density perturbation following a fluid particle is given by

$$\frac{\mathrm{d}}{\mathrm{d}t}\rho'\langle t\rangle = -\frac{\partial\overline{\rho}}{\partial z}w\langle t\rangle + \kappa\nabla^2\rho'\langle t\rangle, \tag{2.3}$$

where the notation $\langle t\rangle$ is used to denote coordinates following a fluid particle. The local divergence of the diapycnal flux, $\kappa\nabla^2\rho'\langle t\rangle$, gives the rate at which the fluid particle is changing its density owing to small-scale mixing: we refer to this as the *Lagrangian mixing rate*. One of the key objectives of this work was to study the characteristics and time history of the mixing following fluid particles. As noted in § 1, this seems to be fundamental to the detailed understanding of mixing and dispersion in stratified flows. Note that in a fully turbulent flow the magnitude of the Lagrangian mixing rate should not depend directly on the molecular diffusivity since the turbulence generates scales that are sufficiently small for molecular diffusion to balance advection.

Integrating (2.3) with respect to time with the initial condition $\rho'\langle 0\rangle = 0$ yields

$$\rho'\langle t\rangle = -\frac{\partial\overline{\rho}}{\partial z}\,z\langle t\rangle + \Delta\rho\langle t\rangle, \tag{2.4}$$

where $z\langle t\rangle$ is the vertical particle displacement relative to its initial position, and the change in density of the fluid particle $\Delta\rho\langle t\rangle$ is given by

$$\Delta\rho\langle t\rangle = \int_0^t \kappa\nabla^2\rho'\langle\tau\rangle\,\mathrm{d}\tau. \tag{2.5}$$

Equation (2.4) shows that fluid particle displacements $z\langle t\rangle$ may be considered to comprise an *'isopycnal'* component $z_i = -\rho'/(\partial\overline{\rho}/\partial z)$ and a *'diapycnal'* component $z_* = \Delta\rho/(\partial\overline{\rho}/\partial z)$ with

$$z\langle t\rangle = z_i\langle t\rangle + z_*\langle t\rangle. \tag{2.6}$$

The isopycnal component z_i represents the displacement of a fluid particle from its equilibrium level in the background mean density gradient, i.e. the level where its density matches that of the background. The diapycnal displacement z_* represents a change in the particle equilibrium level owing to changes in its density. The vertical velocity of a fluid particle $w = \mathrm{d}z/\mathrm{d}t$ may similarly be viewed in terms of an isopycnal component $w_i = \mathrm{d}z_i/\mathrm{d}t$ and diapycnal component $w_* = \mathrm{d}z_*/\mathrm{d}t$, where (from (2.3))

$$w\langle t\rangle = w_i\langle t\rangle + w_*\langle t\rangle. \tag{2.7}$$

This decomposition of displacements and velocities into isopycnal and diapycnal components was introduced by PPH and Hunt (1985), and in a more general form by Winters *et al.* (1995, 1996).

Ensemble averaging over all fluid particles, dispersion coefficients associated with the vertical displacements may be defined as

$$K_z = \frac{1}{2}\frac{\mathrm{d}}{\mathrm{d}t}\overline{z^2}\langle t\rangle \;= \overline{zw}\langle t\rangle, \tag{2.8a}$$

$$K_i = \frac{1}{2}\frac{\mathrm{d}}{\mathrm{d}t}\overline{z_i^2}\langle t\rangle = \overline{z_i w_i}\langle t\rangle, \tag{2.8b}$$

$$K_* = \frac{1}{2}\frac{\mathrm{d}}{\mathrm{d}t}\overline{z_*^2}\langle t\rangle = \overline{z_* w_*}\langle t\rangle. \tag{2.8c}$$

Note that it follows from (2.6) and (2.7) that

$$K_z = K_i + K_* + \overline{z_* w_i} + \overline{z_i w_*}\ . \tag{2.9}$$

The turbulent (or advective) density flux may be obtained by multiplying (2.4) by $w\langle t\rangle$ and ensemble averaging to give

$$\overline{\rho' w}\langle t\rangle = -K_z\,(\partial\overline{\rho}/\partial z) + \overline{\Delta\rho\ w}\ . \tag{2.10}$$

Equivalently, using (2.7),

$$\overline{\rho' w}\ \langle t\rangle = \overline{\rho' w_i}\ \langle t\rangle + \overline{\rho' w_*}\ \langle t\rangle = -\left[K_i + K_d\right](\partial\overline{\rho}/\partial z), \tag{2.11}$$

which states that contributions to the flux come from two mechanisms. The first is associated with the (reversible) displacement of isopycnals and is given by the isopycnal dispersion coefficient K_i, i.e. $\overline{\rho' w_i} = -K_i\ (\partial\overline{\rho}/\partial z)$; the second is associated with the (irreversible) diapycnal displacements z_* that arise from changes to the density of fluid particles owing to small-scale mixing. This contribution to the flux is given by a diapycnal diffusivity K_d, i.e. $\overline{\rho' w_*} = -K_d\ (\partial\overline{\rho}/\partial z)$, where $K_d = \overline{z_i w_*}$ is related to the scalar dissipation rate by

$$K_d = \frac{\epsilon_\rho}{(\partial\overline{\rho}/\partial z)^2}, \tag{2.12}$$

with

$$\epsilon_\rho = -\kappa\ \overline{\rho'\nabla^2\rho'} = \kappa\ \overline{\nabla\rho'\cdot\nabla\rho'}. \tag{2.13}$$

Winters & D'Asaro (1996) derived an exact expression relating diapycnal flux to the mean square density gradients averaged over isopycnal surfaces. Their derivation used a reference state for the density field where all fluid particles are adiabatically rearranged to their equilibrium positions, i.e. to a state of minimum potential energy (see also Winters *et al.* 1995). In the present case, this reference state is the background mean density field which does not change because the flow is homogeneous with a uniform diapycnal flux that is divergence free. Furthermore, statistical homogeneity also implies that averages over isopycnal surfaces are formally equivalent to volume averages. The diapycnal diffusivity derived by Winters & D'Asaro (1996) simplifies to (2.12) in this case.

Note that the diapycnal diffusivity $K_d = \overline{z_i w_*}$ is not in general equal to the diapycnal dispersion coefficient $K_* = \overline{z_* w_*}$ defined above (equation (2.8*c*)). However, if the isopycnal displacements (due to advection) and the diapycnal displacements (due to small-scale mixing) are statistically independent, i.e. $\overline{z_i z_*} = 0$, and if the integrated changes in the fluid particle densities are independent of the velocity, i.e. $\overline{\Delta\rho\ w} = 0$, then it follows that $K_d = K_*$. Both conditions are expected to be true for high Re number turbulent flows where there is large separation between the advective and diffusive scales. For example, Pope (1998) analysed the effects of molecular diffusivity on turbulent mixing of passive scalars. He showed that if the scalar flux is independent of the molecular diffusivity, as suggested by experiments and DNS at high Reynolds and Péclet numbers, then the Lagrangian mixing rate must be independent of the velocity, which implies $\overline{\Delta\rho\ w} = 0$.

For a transient turbulent mixing event (as considered here), the buoyancy flux $(g/\rho_0)\overline{\rho' w}$ can be integrated over the duration of the event $t = 0 \to \infty$ to give (using

(2.10))

$$B = N^2 \tfrac{1}{2}\overline{z^2}\langle\infty\rangle + \int_0^\infty \frac{g}{\rho_0}\overline{\Delta\rho\ w}\langle t\rangle\,\mathrm{d}t, \tag{2.14}$$

where it follows from (2.6) after putting $\rho'\langle\infty\rangle = z_i\langle\infty\rangle = 0$, that

$$\overline{z^2}\langle\infty\rangle\ = \overline{z_*{}^2}\langle\infty\rangle. \tag{2.15}$$

The ratio of the integrated buoyancy flux B to the initial turbulent kinetic energy defines a mixing efficiency for the transient mixing event and represents the proportion of the initial kinetic energy that goes into doing work against buoyancy forces (Stretch *et al.* 2001). The relationship between the mixing efficiency and the strength of the stratification is important for quantifying the effects of episodic mixing events in geophysical flows (e.g. Linden 1979; Gregg 1987). Equations (2.14) and (2.15) indicate that the mixing efficiency is related to the asymptotic diapycnal displacements of fluid particles to new equilibrium positions within the background mean density gradient. In stably stratified flows, if small-scale mixing were absent ($\Delta\rho = 0$) then $\overline{z^2}\langle\infty\rangle$ would be zero since all fluid particles would be driven by buoyancy forces to ultimately return to their original equilibrium levels. The mixing efficiency would therefore also be zero.

3. Methods

3.1. *Eulerian velocity field*

The numerical simulations described here were carried out using the pseudo-spectral DNS code described by Riley, Metcalfe & Weissman (1981). The DNS code simulates a flow field that is periodic in all three spatial coordinates, with constant background density gradient. Simulations were performed at resolutions ranging from 32^3 to 128^3, but all the results reported here were obtained at 64^3.

For all numerical experiments, the turbulent flow field was initialized as a Gaussian, isotropic and solenoidal velocity field in the usual way using random Fourier modes with a specified energy spectrum. The initial energy spectrum had an exponential form (see e.g. Townsend 1976):

$$E(k) = C\,u_0^2\,L_0^5\,k^4 \exp\left[-\tfrac{1}{2}k^2L_0^2\right],$$

where C is a constant scaling factor, and u_0 and L_0 are initial velocity and length scales of the turbulence. This spectrum has its peak energy at wavenumbers $kL_0 = 2$. The Reynolds number for all 64^3 simulations was $Re = u_0L_0/\nu = 200$. The Prandtl (or Schmidt) number was $Pr = \nu/\kappa = 0.5$ in order to ensure accurate resolution of the smallest scales of the density field, although some simulations at $Pr = 1$ were also carried out.

The stable stratification can be characterized by the initial Richardson number, defined as $Ri = (NL_0/u_0)^2$, which was varied in the range $0 < Ri < 1000$. Note that there are two time scales imposed on the flow, the initial turbulence time scale L_0/u_0 and the buoyancy time scale N^{-1}. The ratio of these time scales is $Ri^{1/2}$.

For all simulations, the initial energy was exclusively kinetic in form, i.e. the initial density fluctuations (and hence PE_0) were set to zero. The turbulence was then allowed to decay until at least 90% of the initial turbulence energy had dissipated. Decay times of ten times the initial time scale of the turbulence L_0/u_0 were used.

Numerical experiments were also carried out using an alternative initialization procedure where the flow was allowed to evolve, without any buoyancy effects, to

time $u_0 t/L_0 = 1$. The scalar fluctuations were then set to zero before restarting the simulations with buoyancy effects turned on. This procedure, also used by Kimura & Herring (1996) and Metais & Herring (1989), is intended to allow the nonlinear transfer to small scales to develop prior to the sudden introduction of the stratification. Results from these simulations (e.g. the evolution of the energy and fluxes) were at least qualitatively similar to those in which the stratification was introduced at $t = 0$. It was decided to use the $t = 0$ initialization for the main set of numerical experiments because the initial spectrum is more precisely defined and repeatable at different resolutions and Reynolds numbers. A similar approach was used by Kaneda & Ishida (2000). We note that neither of these initialization schemes is a precise representation of physically realizable flows, such as in laboratory experiments using grid-generated turbulence with salt or heat stratified fluids. Nevertheless, comparison between DNS and such experiments (e.g. Metais & Herring 1989) has indicated satisfactory general agreement.

The initial velocity scale u_0, length scale L_0, and density scale $L_0|\partial\overline{\rho}/\partial z|$ are used to non-dimensionalize the results presented in this paper.

3.2. *Particle tracking*

In order to gather Lagrangian statistics, a particle-tracking algorithm was incorporated into the DNS code of Riley *et al.* (1981). Given an evolving three-dimensional periodic turbulent velocity field at discrete collocation (grid) points (available from the Eulerian DNS), an interpolation scheme was required to determine the velocity at any arbitrary position within the field. A cubic spline scheme was selected for this study, and follows the formulation of Yeung & Pope (1988). It is fourth-order accurate and provides twice-continuously differentiable approximations.

Using the interpolation scheme, the advection tracks of fluid particles can be computed from a set of initial starting positions by numerical integration. Denoting $\boldsymbol{x}\langle t \rangle$ and $\boldsymbol{u}\langle t \rangle$ as the position and velocity at time t of a fluid particle with initial position $\boldsymbol{x}\langle 0 \rangle$ at time $t = 0$, the equation of motion of the particle is

$$\frac{\mathrm{d}\boldsymbol{x}\langle t \rangle}{\mathrm{d}t} = \boldsymbol{u}\langle t \rangle, \tag{3.1}$$

where the Lagrangian velocity $\boldsymbol{u}\langle t \rangle$ is related to the Eulerian velocity $\boldsymbol{u}(\boldsymbol{x}, t)$ by

$$\boldsymbol{u}\langle t \rangle = \boldsymbol{u}(\boldsymbol{x}\langle t \rangle, t).$$

Particle positions are obtained by integrating (3.1) in time using a second-order accurate Adams–Bashforth scheme. The time step was the same as for the Eulerian simulation.

Both Lagrangian velocities and densities were interpolated at each time step of the simulations. The mixing following the fluid particles was not directly interpolated, but was inferred from (2.3).

A total of 512 particles was tracked in each simulation. They were initially distributed onto an 8^3 equi-spaced cubic sub-lattice of the full computational domain. The initial spacing between particles was therefore about $0.7L_0$.

3.3. *Statistical averaging*

All the Eulerian statistics that are reported here are volume averages over the computational domain. All Lagrangian statistics are ensemble averages over the full set of particles used in the simulations (i.e. 512 particles in this case). We note that, for a statistically homogeneous flow field, single time Eulerian and Lagrangian statistics

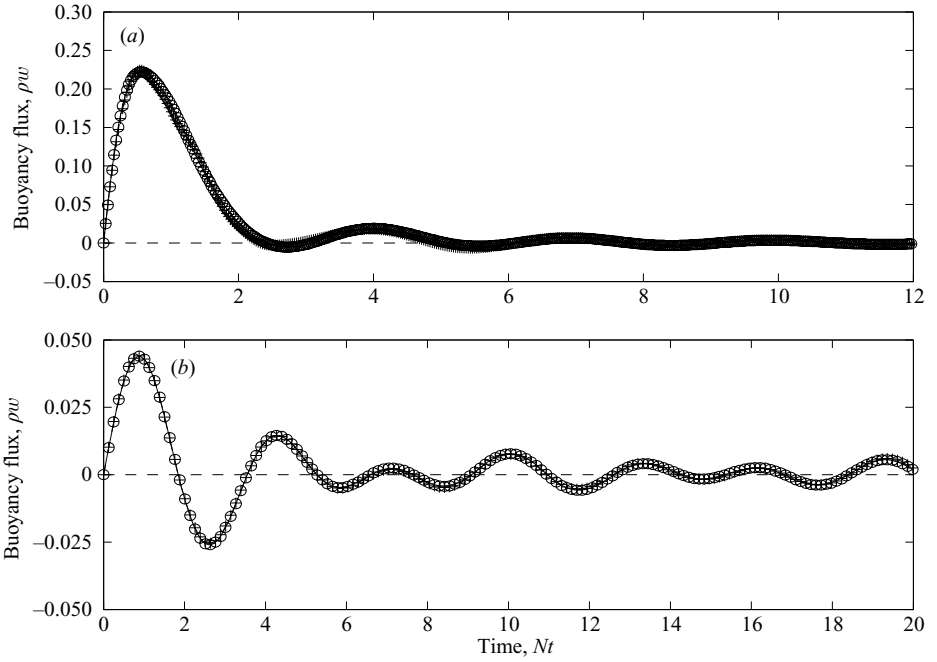

FIGURE 1. Comparison of ○, Eulerian and +, Lagrangian averages of the buoyancy flux for (*a*) $Ri = 1.58$, and (*b*) $Ri = 158$.

are formally equivalent. A comparison of Eulerian and Lagrangian averages for the buoyancy flux is shown in figure 1 where it can be seen that they are closely matched (as required). This indicates that the sample size of 512 particles, while relatively small, is sufficient for obtaining accurate second-order statistics, i.e. to within about 5% of their Eulerian counterparts.

4. Results and discussion

4.1. *Flow energetics*

In this section, we present a brief discussion on the flow energetics (Eulerian statistics) of these stably stratified flow simulations in order to highlight some key features of the flow evolution and to establish that the results from the present simulations are not significantly different to those previously obtained from DNS of decaying stratified turbulence (Riley *et al.* 1981; Metais & Herring 1989; Kimura & Herring 1996).

Figure 2 shows the behaviour of kinetic energy, potential energy and total energy for $Ri = (1.58, 10 \text{ and } 158)$ with corresponding Brunt–Väisälä period T_{BV} of 5, 2 and 0.5, respectively, non-dimensionalized by L_0/u_0. In all the cases, the potential energy is initially zero, but grows rapidly (especially in the high Ri cases) and peaks at approximately $T_{BV}/6$. The potential energy then decays while oscillating at about half the Brunt–Väisälä period. The kinetic energy initially reduces more rapidly for the strongly stable cases (e.g. $Ri = 158$) owing to the faster conversion of kinetic energy to potential energy. However, this process is reversed soon after the peak in potential energy occurs (see figure 2*c*). At this stage, the kinetic energy can increase because of an exchange between potential energy and vertical kinetic energy, before continuing to decay to almost zero at times of order $10L_0/u_0$.

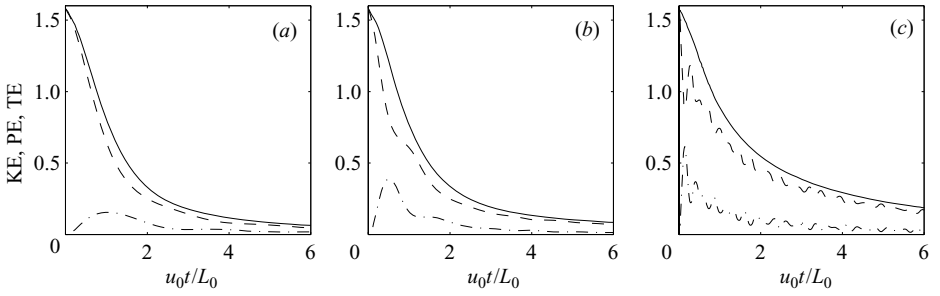

FIGURE 2. The kinetic energy, KE (dashed lines); the potential energy, PE (dash-dotted lines); and the total energy, TE (solid lines); as a function of time u_0t/L_0 for (*a*) $Ri = 1.58$, (*b*) 10, and (*c*) 158, respectively.

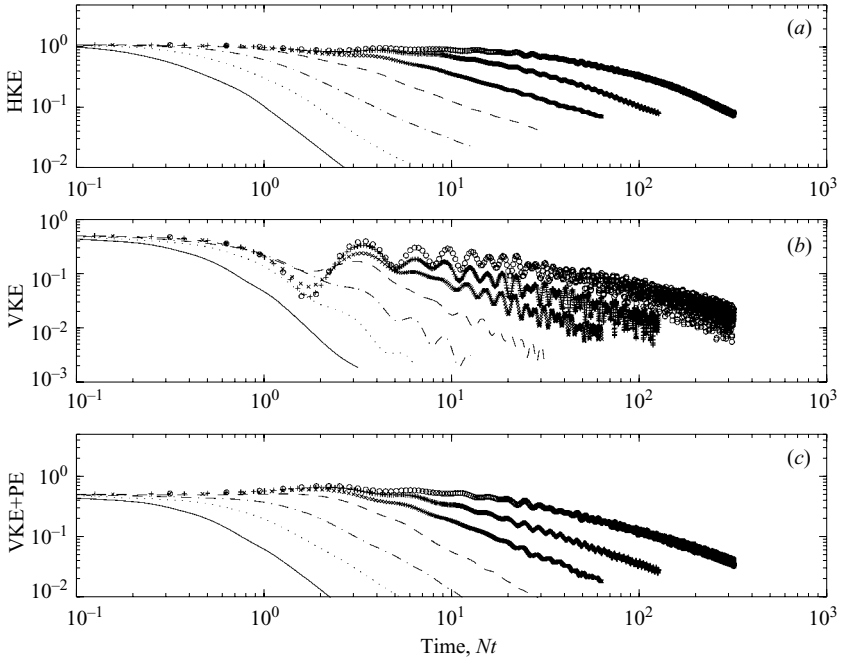

FIGURE 3. The evolution of (*a*) the horizontal kinetic energy (HKE), (*b*) the vertical kinetic energy (VKE) and (*c*) the sum of vertical kinetic energy plus potential energy (VKE + PE) versus Nt. The Richardson numbers corresponding to the lines in each plot are (left to right) $Ri = 0.10,\ 0.39,\ 1.58,\ 10,\ 39.5,\ 158$ and 1000.

The evolution of the horizontal kinetic energy (HKE), the vertical kinetic energy (VKE), and combined potential energy (PE) and VKE are shown in figure 3 as a function of Nt. The evolution of HKE shows relatively small differences with changing Ri. In contrast, the evolution of VKE shows the effects of an emergent internal wave field for the high Ri flows and for times $Nt \gtrsim 2\pi$. The oscillations in the VKE (at about twice the buoyancy frequency) are due mainly to exchanges between VKE and PE, and are therefore not evident in the plots of (VKE + PE) and HKE. This suggests a decoupling of the vertical (internal wave) motion from the horizontal modes, an observation made previously by Riley *et al.* (1981) and Metais & Herring (1989).

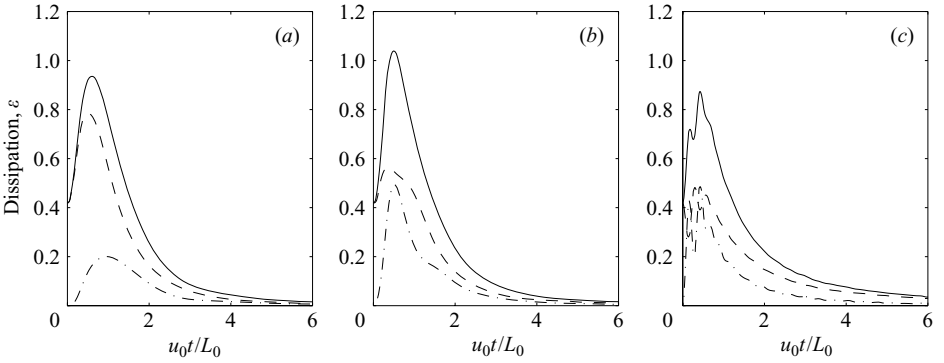

FIGURE 4. The dissipation of kinetic energy, KE (dashed lines) potential energy, PE (dash-dotted lines) as a function of time u_0t/L_0 for (*a*) $Ri = 1.58$, (*b*) 10 and (*c*) 158, respectively.

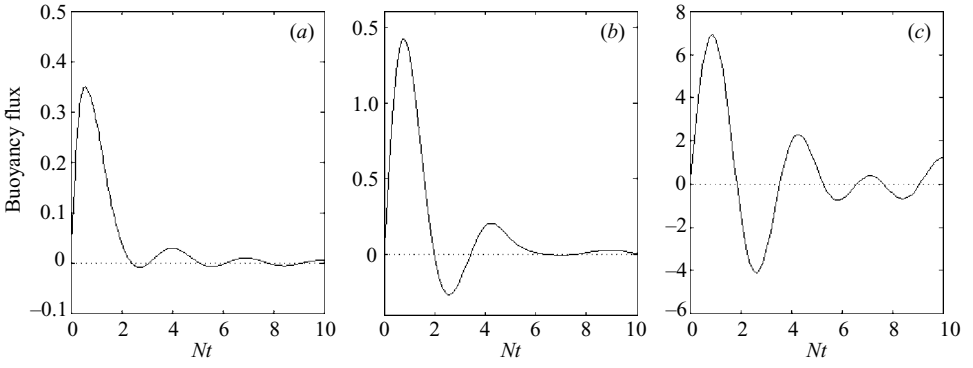

FIGURE 5. Buoyancy flux as a function of time Nt for (*a*) $Ri = 1.58$, (*b*) 10 and (*c*) 158, respectively.

Note that for large times, the total energy remaining in the flow is slightly higher for the more strongly stratified cases (refer to figure 2) indicating a (small) overall reduction in dissipation as the stratification strengthens. Integrated over the full duration of the simulations, $0 \leqslant u_0t/L_0 \leqslant 10$, the change in the total dissipation between $Ri = 0$ and $Ri = 1000$ is less than 10%. However, the temporal distribution of the dissipation is altered by the stratification with dissipation rates tending to be higher than the unstratified case for times $Nt \lesssim 2\pi$, but lower for times $Nt \gtrsim 2\pi$. The relative insensitivity of dissipation to the stratification strength has been noted previously by Riley *et al.* (1981) and others, and is discussed in some detail by Hanazaki & Hunt (1996).

The contributions to the total energy dissipation from the dissipation of kinetic and potential energy are shown in figure 4 for $Ri = 1.58$, 10 and 158. As the stratification becomes stronger, the contribution from the potential energy dissipation ϵ_{PE} becomes a significant proportion of the total energy dissipation ϵ. Integrated over the duration of the simulations, this proportion reaches about 30%.

Figure 5 shows the evolution of the buoyancy flux $(g/\rho_0)\overline{\rho' w}$ for $Ri = 1.58$, 10 and 158 as a function of non-dimensional time Nt. The flux grows rapidly (it is initially zero in these simulations) and peaks at $Nt \simeq 1$ which is also when the potential energy peaks. It then reduces to zero at times $Nt \simeq 2$, and in the more strongly stable cases,

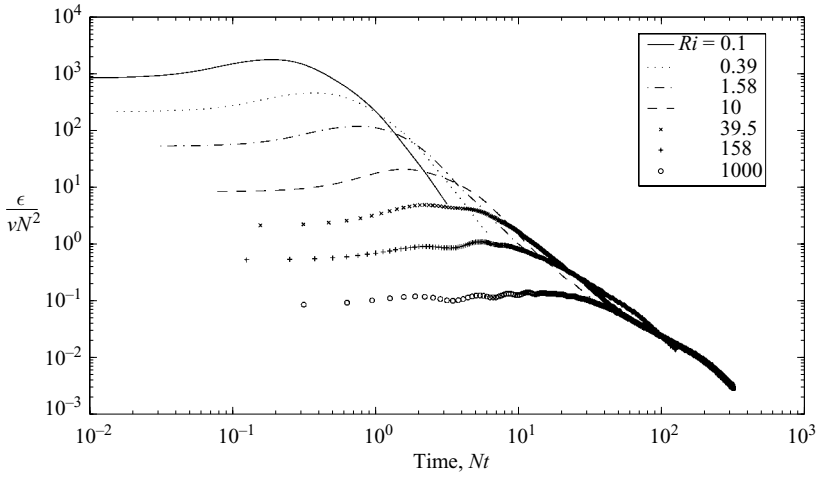

FIGURE 6. Turbulence activity parameter $\epsilon/\nu N^2$ as a function of time, Nt.

changes sign and oscillates about zero with a period of about half the buoyancy period. This process is physically established when fluid particles have converted their vertical kinetic energy to potential energy, and start migrating back towards their equilibrium levels, thereby reconverting their potential energy back into kinetic energy. These 'wavelike' features of the flux evolution have been previously shown (Hunt, Stretch & Britter 1988; Hanazaki & Hunt 1996; Kaneda & Ishida 2000) to be reproduced by linear theory.

Shih *et al.* (2005) used results from a large number of simulations of homogeneous, sheared, stratified turbulence to show that the turbulence activity parameter $\epsilon/\nu N^2$ may be used to parameterize the turbulent diffusivity in these flows. This parameter is also widely used for mixing estimates in geophysical flows. Shih *et al.* suggest three regimes: a diffusive regime ($\epsilon/\nu N^2 < 7$); an intermediate regime ($7 < \epsilon/\nu N^2 < 100$); and an energetic regime ($\epsilon/\nu N^2 > 100$). In the diffusive regime, turbulence and mixing are weak and diffusivities approach molecular values. In the intermediate and energetic regimes, diffusivities increase with $\epsilon/\nu N^2$. Observed values in the ocean thermocline are typically in the intermediate range.

The evolution of $\epsilon/\nu N^2$ for the present simulations are shown plotted in figure 6. For the lower Ri cases, values start in the energetic or intermediate regimes and decay as the flow evolves. However, for the most stable cases ($Ri \gtrsim 40$), the values are within the diffusive regime for the entire duration of the simulations. Therefore only weak mixing is anticipated in these cases.

4.2. *Lagrangian displacements*

In figure 7, sample three-dimensional particle tracks for $Ri = 0.39, 1.58, 10$ and 158 are shown. The shading of the particle tracks indicates the local rate of mixing $\kappa\nabla^2\rho'(t)$. The tracks for the low Ri flows show how the particles wander with freedom in all three spatial directions. On the other hand, in the strongly stable case ($Ri = 158$), the particle is more or less restricted to a horizontal plane with small vertical oscillations at approximately the Brunt–Väisälä period $T_{BV} = 2\pi/N$. This corroborates the speculation that the vertical motions of these strongly stable flows may be characterized as linear internal waves.

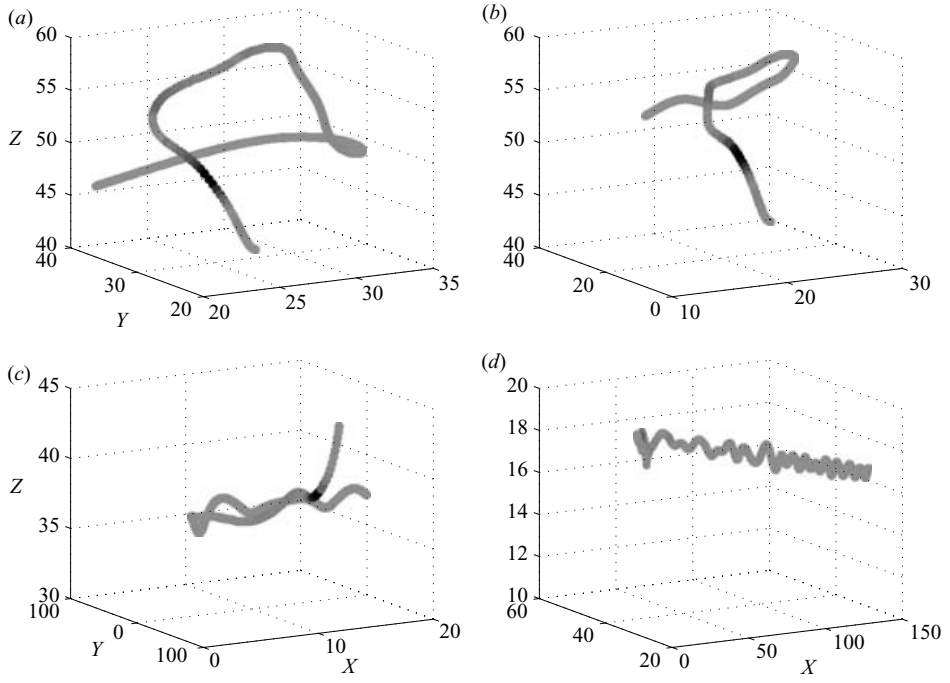

FIGURE 7. Sample particle tracks at (*a*) $Ri = 0.39$; (*b*) $Ri = 1.58$; (*c*) $Ri = 10$; (*d*) $Ri = 158$. The grey scale of the tracks indicates the relative magnitude of the local mixing rate with lowest values grey and highest values black.

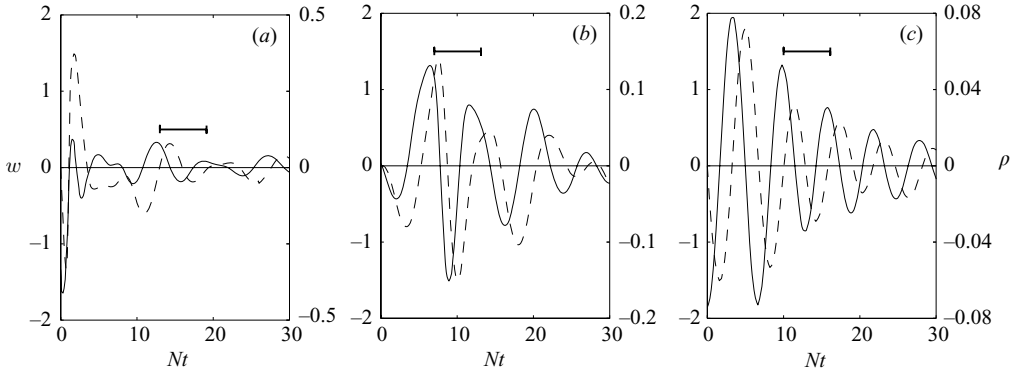

FIGURE 8. Time histories of w (solid lines) and ρ' (dashed lines) for (*a*) $Ri = 10$; (*b*) $Ri = 158$; (*c*) $Ri = 1000$. The width of the horizontal bars shown corresponds to one Brunt–Väisälä period, $T_{BV} = 2\pi/N$.

To further elucidate this, we plotted some sample time histories of the vertical velocity w and density fluctuations ρ' of particles for $Ri = 10$, 158 and 1000, as shown in figure 8. The time series show that for $Nt \gtrsim 2\pi$ both w and ρ' oscillate with periods of order T_{BV}, and that ρ' is 90° out of phase with w. This clearly indicates the emergence of linear internal wave motions for $Nt \gtrsim 2\pi$, especially for the strongly stable cases ($Ri = 158$, 1000).

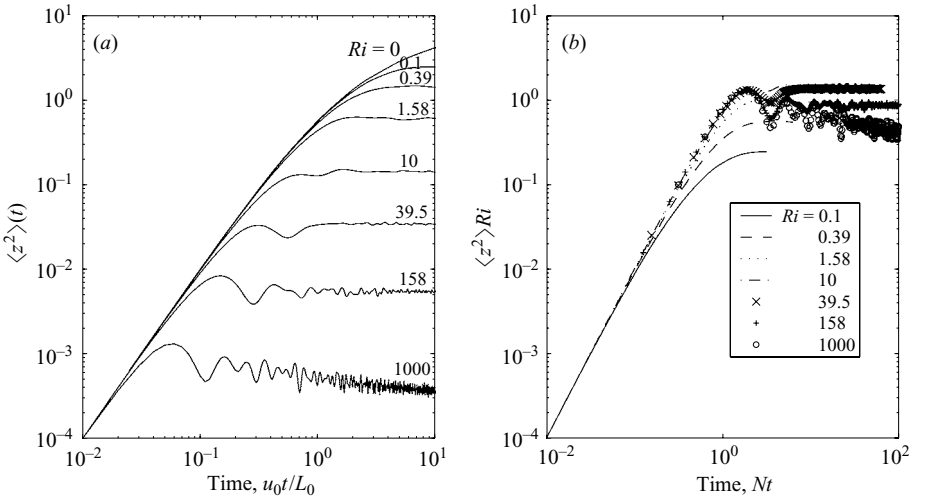

FIGURE 9. (*a*) Mean square vertical displacements as a function of time, $u_0 t/L_0$; and (*b*) normalized mean square vertical displacement as a function of time, Nt.

The mean square vertical displacements, $\overline{z^2}\langle t\rangle$, of particles from their initial positions are shown in figure 9(*a*) as a function of time $u_0 t/L_0$ and for various Ri values. The displacement variances grow initially, but when $Ri > 0$, they level off to near constant values that scale approximately as Ri^{-1}. Figure 9(*b*) shows the same data, scaled with Ri, and plotted as a function of non-dimensional time Nt. Note that $\overline{z^2}\langle t\rangle$ starts to level off at $Nt \simeq 2$, which is when the buoyancy fluxes reduce to zero (refer to figure 5). The displacement statistics plotted with this scaling collapse well at small times and stay together to within about a factor of two for large times.

In the case of the strongest stratifications (e.g. $Ri = 1000$), the mean square displacements reduce slightly at large times. This is associated with residual density fluctuations that relax at long time scales as fluid particles gradually re-settle to their equilibrium levels within the density gradient, a process that gives rise to a counter-gradient flux. Hanazaki & Hunt (1996) discussed the presence of sustained counter-gradient fluxes in these flows, and noted that they depend on the Prandtl number of the fluid and that less diffusive scalars can result in stronger counter-gradient fluxes at small scales.

The growth of the r.m.s. vertical displacements for small times is consistent with the initial Taylor range, $\sigma_z\langle t\rangle \sim t$ for all Ri in our simulations. For the unstratified case ($Ri = 0$), the growth is $\sigma_z\langle t\rangle \sim t^{1/2}$ at long times, consistent with Taylor's theory for stationary turbulence, although in this case the turbulence is decaying. We observe that there is no $t^{1/2}$ growth at long times for any of the $Ri \geq 0$ cases.

The mean square horizontal displacements $\overline{x^2}\langle t\rangle$ and $\overline{y^2}\langle t\rangle$ shown in figure 10 indicate that stable stratification has only small effects on the particle displacements in the horizontal plane. In fact, the horizontal displacements are slightly enhanced with increasing stratification. Therefore, at large times, there are residual horizontal motions present in these strongly stratified flows that are growing in scale more rapidly than in more weakly stratified cases.

The displacement statistics discussed above are consistent with those previously presented by Kimura & Herring (1996) and Kaneda & Ishida (2000).

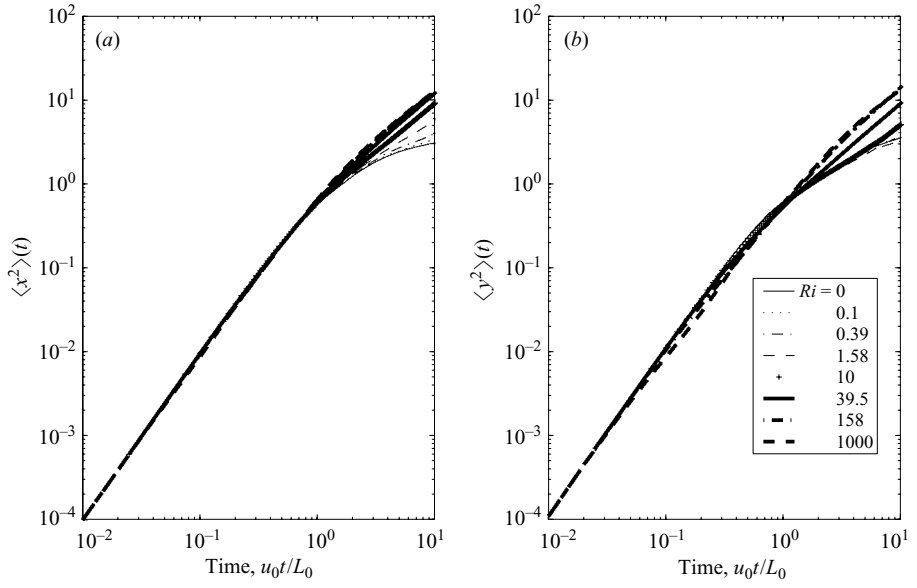

FIGURE 10. Mean square horizontal displacements as a function of time, u_0t/L_0 and for $Ri = 0$, 0.10, 0.39, 1.58, 10.0, 39.5, 1000.

4.3. *Lagrangian mixing*

The results discussed in §§ 4.1 and 4.2 are similar to those previously reported by Riley *et al.* (1981), Metais & Herring (1989), Kimura & Herring (1996), or Kaneda & Ishida (2000). In this section, we focus on the novel contribution of the present work, namely our results concerning the mixing following fluid particles. Recall from § 2.2 that the Lagrangian mixing rate is defined as the rate at which fluid particles are changing their density and is given by the local divergence of the diapycnal flux following the particles, i.e. $\mathrm{D}\rho/\mathrm{D}t = \kappa\nabla^2\rho$.

4.3.1. *Spatio-temporal characteristics*

The evolution of the mean square Lagrangian mixing rates are shown plotted in figure 11 as a function of time. It can be seen how average mixing rates initially increase rapidly from their zero initial values to peak at times of order $u_0t/L_0 \simeq 1$ or less, before decaying approximately exponentially down to negligibly small values at $u_0t/L_0 = 10$. When the time axis is re-scaled using the buoyancy frequency N, as shown in figure 11(*b*), it is evident that the mixing rates tend to collapse to small values at times $2\pi \leqslant Nt \leqslant 4\pi$, i.e. between one and two buoyancy periods $T_{BV} = 2\pi/N$ after initializing the flow. We later show (§ 4.4) that this is also the time when overturning motions disappear from the flow.

Sample time histories of the mixing following fluid particles are shown in figure 12, together with corresponding time series for the density perturbations. It can be seen that the mixing is temporally intermittent. That is, for this transient (decaying) turbulent flow, most of the mixing for individual fluid particles seems to occur during a small number of intense short-lived events, so that the residence time of particles in regions where there is intense mixing is small. This is also evident in the sample time histories shown in figure 7.

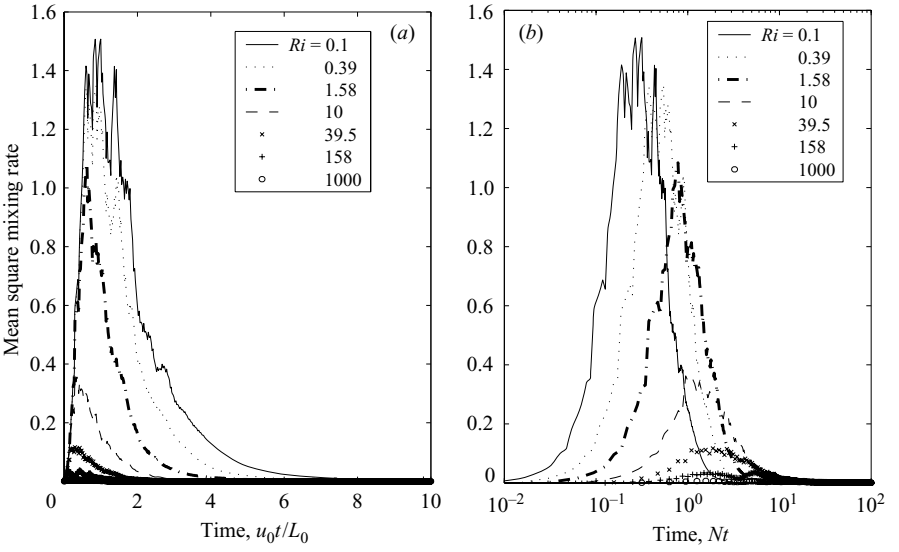

FIGURE 11. Mean square Lagrangian mixing rates for a range of Ri numbers (a) as a function of time tu_0/L_0; and (b) as a function of Nt.

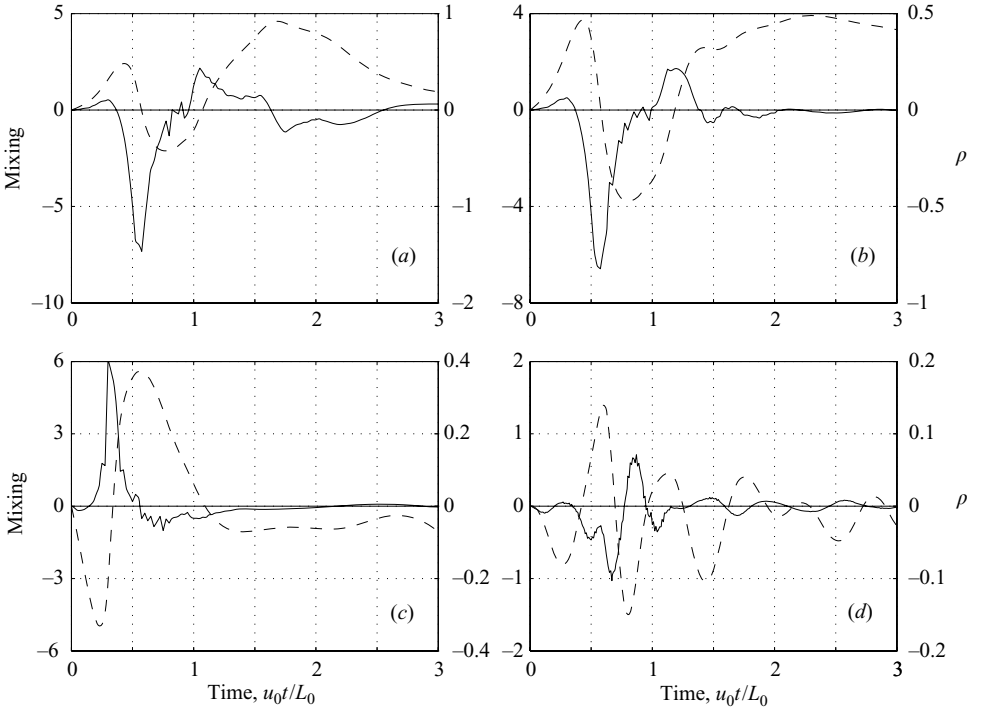

FIGURE 12. Sample time series of Lagrangian mixing (solid lines) and density perturbations (dashed lines) following fluid particles for (a) $Ri = 0.39$, (b) 1.58, (c) 10 and (d) 158.

Mixing rates are also spatially intermittent. Probability distributions of mixing rates during the intense mixing phase of the flow ($Nt \leqslant 2\pi$, see figure 11) are non-Gaussian with kurtosis excess in the range 10–40 (decreasing for stronger stratifications).

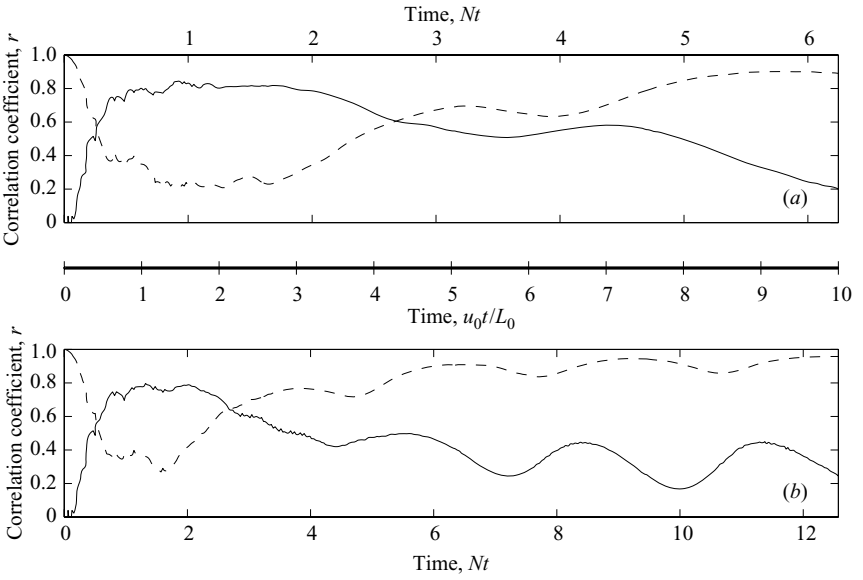

FIGURE 13. Correlation between $\mathrm{d}\rho'/\mathrm{d}t$ and mixing rates (solid lines) and vertical velocity (dashed lines) for (*a*) $Ri = 0.39$, (*b*) $Ri = 10$.

From (2.3), it can be seen that changes to the density perturbation following fluid particles have a contribution from both the stirring action of the vertical motion within the background mean density gradient, and from small-scale mixing. The sample time histories in figure 12 indicate that the latter can dominate the changes in the density perturbations of fluid particles during the mixing phase of the flow. The density perturbations shown in figure 12 are non-dimensionalized by the scale $L_0|\partial\overline{\rho}/\partial z|$. It is therefore evident from the samples shown in figure 12 that episodic intense mixing events can produce sudden density changes that are equivalent in magnitude to that from a vertical displacement of order L_0 within the background density gradient.

To further illustrate the relative roles of 'stirring' and 'mixing' in changing the density perturbations of fluid particles, ensemble-averaged cross-correlations between the changes in density perturbations $\mathrm{d}\rho'/\mathrm{d}t$ (the term on the left-hand side of (2.3)) and the vertical velocities and mixing rates (representing the two terms on the right-hand side of (2.3)) are shown in figure 13 for two different Ri numbers. Disregarding the initial transient which is an artefact of the initial conditions used for the simulations, it can be seen that the relative importance of 'stirring' and 'mixing' changes during the evolution of the flow. During the intense mixing phase of the flow ($Nt < 2\pi$), the instantaneous density variations are driven by the small-scale mixing processes, with stirring having a relatively smaller role. However, as mixing rates reduce ($Nt \simeq 2\pi$), the roles gradually reverse and at larger times ($Nt > 4\pi$), the rate of change of the density perturbation following fluid particles becomes nearly perfectly correlated with their vertical velocities. The latter is consistent with internal wave kinematics, where fluid particles are oscillating about their equilibrium level within the background (linear) density profile, but with irreversible mixing essentially absent (see also figure 8).

In the $Ri = 0$ case (not shown here), the correlations between $\mathrm{d}\rho'/\mathrm{d}t$ (where ρ is interpreted as a passive scalar concentration in this case) and the mixing remain consistently high ($\simeq 0.8$) for the duration of the simulation. The corresponding

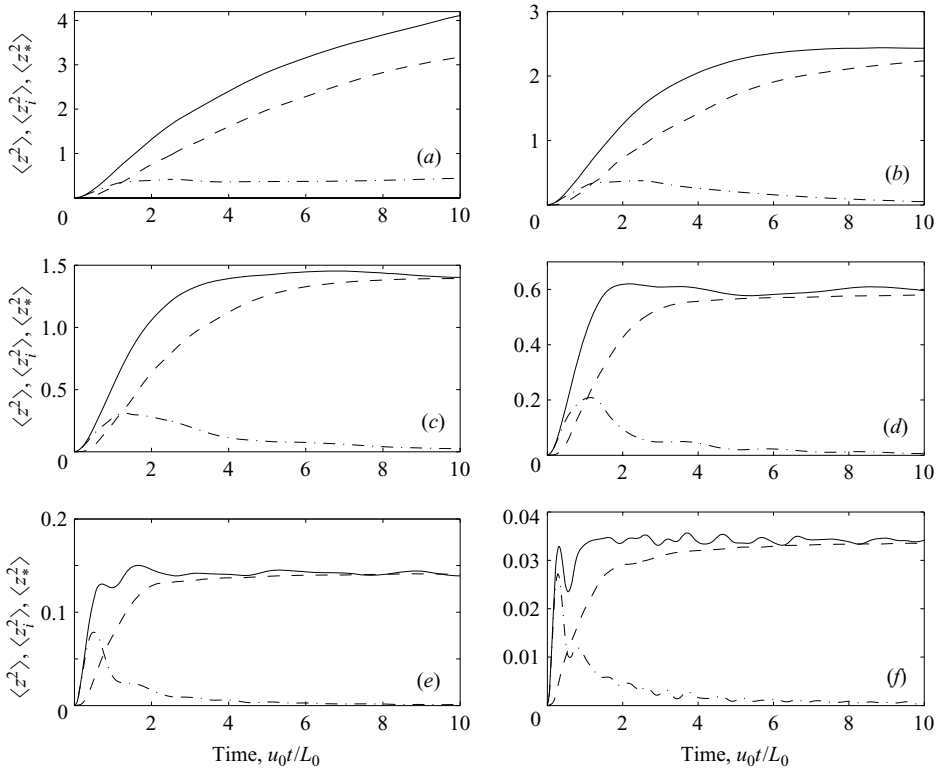

FIGURE 14. Components of the mean square vertical displacements of fluid particles as a function of time: total displacements (solid lines), diapycnal displacements (dashed lines), and isopycnal displacements (dashed-dotted lines). (*a*) $Ri = 0$; (*b*) $Ri = 0.1$; (*c*) $Ri = 0.39$; (*d*) $Ri = 1.58$; (*e*) $Ri = 10$; (*f*) $Ri = 39.5$.

correlations between $\mathrm{d}\rho'/\mathrm{d}t$ and the vertical velocities are much smaller ($\simeq 0.2$) and also remain approximately constant during the simulation.

4.3.2. *The role of Lagrangian mixing in the density flux*

One of the key questions of this investigation concerns the role of small-scale mixing in the density (or buoyancy) flux. As noted in § 2.2, it has been speculated that small-scale mixing becomes increasingly important as the stratification strengthens because of the constraints on vertical particle displacements. The simulations allow this supposition to be tested directly.

The role of Lagrangian mixing can be analysed by considering the relative magnitude of the isopycnal and diapycnal displacements as defined in § 2.2. Figure 14 shows the evolution of the mean square displacement components with time for various Ri numbers.

Consider first the $Ri = 0$ case where the density is a passive scalar marker with no dynamical effects on the turbulence or on the dispersion process. Fluid particles are initially advected away from their starting positions (where their densities match the background mean values) without changing their densities (i.e. the Lagrangian mixing is initially zero). During this initial transient, the isopycnal displacement component dominates. However, by time $u_0t/L_0 = 1$, the diapycnal displacements due to mixing have become significant, while the mean square isopycnal displacements

reach a maximum and stabilize at nearly constant values for times $u_0 t/L_0 > 2$. The mean square diapycnal displacements continue to grow and become the dominant contributor to the total mean square particle displacements. Physically, the Lagrangian mixing causes the density of fluid particles to relax towards the local background mean value at a rate that strongly limits the density perturbations that they carry, even though the displacements from their original positions become large in this case. In other words, mixing changes the densities of fluid particles in a manner that limits any 'memory' of their density marking. If mixing were absent, the diapycnal displacement component would remain zero, and the isopycnal displacements (and associated density fluctuations) would grow with time since the fluid particles retain their initial density.

Turning to the $Ri > 0$ cases shown in figure 14, it can be seen that there are two fundamental ways in which the stratification affects the evolution of the fluid particle displacements. The most obvious effect, as already noted in § 4.2, is the strong suppression of the total mean square vertical displacements which cease to grow for times $Nt \gtrsim 2$ and reach approximately constant values that scale inversely on the strength of the stratification (note the different vertical scales in figure 14). Secondly, the contributions from the isopycnal and diapycnal displacements change as Ri increases. The mean square isopycnal displacements grow initially as in the $Ri = 0$ case, but reach a well-defined peak at times corresponding to $Nt \simeq 2$ before subsequently decaying to zero at later times. The mean square diapycnal displacements also initially grow as in the $Ri = 0$ case, but then level off at times corresponding to between one and two buoyancy periods. At these and later times, the diapycnal component accounts for nearly all of the total fluid particle displacements. Physically, small-scale mixing changes the equilibrium level of the fluid particles, but as Ri increases, the mixing is strongly suppressed which in turn limits these changes. As the energy of the flow dissipates, fluid particles are driven by buoyancy forces to settle into their new equilibrium levels.

The dispersion coefficients K_z, K_i and K_* associated with the displacement statistics (equation (2.8)) are shown in figure 15 as a function of time and for various Ri numbers. The diapycnal diffusivity K_d is also shown for each case. (Note that the 'noise' in the computed K_* values are statistical sampling errors associated with the small number of particles used for the ensemble averages.)

It can be seen that K_z provides a poor indication of the diapycnal diffusivity in all cases, even for $Ri = 0$. As Ri increases, K_z is strongly suppressed for times corresponding to $Nt \gtrsim 2$, and starts oscillating about zero. These effects on K_z are associated with the attenuated growth in the mean square vertical displacements. Furthermore, the isopycnal dispersion coefficient K_i gives a negative and oscillatory contribution to K_z as Ri increases. The oscillations in K_i are linked to the buoyancy frequency N and are associated with internal wave motions that do not produce any significant irreversible mixing, i.e. these motions are adiabatic in the sense defined by Winters *et al.* (1995).

The magnitudes of the diapycnal diffusivity K_d and dispersion coefficient K_* are also strongly suppressed as Ri increases, but the effects on their temporal evolution are qualitatively different from those on K_z and K_i. In particular, there are no significant wavelike features in the evolution of K_d and K_*, indicating that the diapycnal mixing is independent of the internal wave motions. The dispersion coefficient K_* is consistently larger than the diffusivity K_d, although the differences become small as Ri increases. As noted in § 2.2, these differences are expected to be small for high-Reynolds-number turbulence.

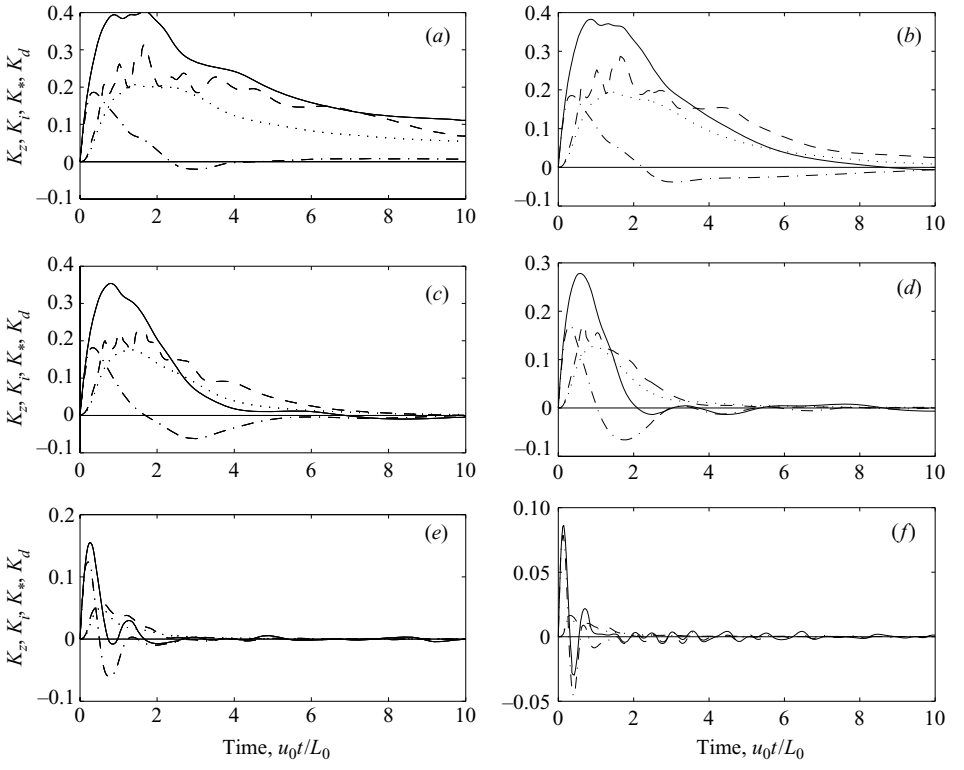

FIGURE 15. Dispersion coefficients associated with vertical fluid particle displacements: total dispersion K_z (solid lines), diapycnal dispersion K_* (dashed lines), and isopycnal dispersion K_i (dashed-dotted lines). The diapycnal diffusivity $K_d = \epsilon_\rho / |\partial \overline{\rho} / \partial z|^2$ is shown as a dotted line. (*a*) $Ri = 0$; (*b*) $Ri = 0.1$; (*c*) $Ri = 0.39$; (*d*) $Ri = 1.58$; (*e*) $Ri = 10$; (*f*) $Ri = 39.5$.

The results reported in this section confirm the notion, highlighted by PPH, that the role of small-scale mixing in changing the density of fluid particles must be properly accounted for in models for diffusion in stably stratified turbulence. The reason for this is that significant reversible (or adiabatic) contributions to the flux can occur in these flows, while it is the irreversible diapycnal contributions to the flux that are most significant in terms of the flow energetics (Winters *et al.* 1995). The latter are entirely due to the effect of small-scale mixing in changing the density of fluid particles.

4.3.3. *Modelling small scale mixing*

The Lagrangian mixing rate was modelled by PPH (following the work of Csanady 1964) with a linear mixing model in the form

$$\kappa \nabla^2 \rho' = -\gamma N \rho', \tag{4.1}$$

where γ is a non-dimensional mixing coefficient. This model assumes that the buoyancy time scale N^{-1} controls the mixing process. The conceptual basis for this supposition (PPH; Hunt 1985) is that strongly stable flows are expected to be dominated by internal wave motions with mixing occurring during rare intermittent events (such as wave 'breaking') that generate local overturning.

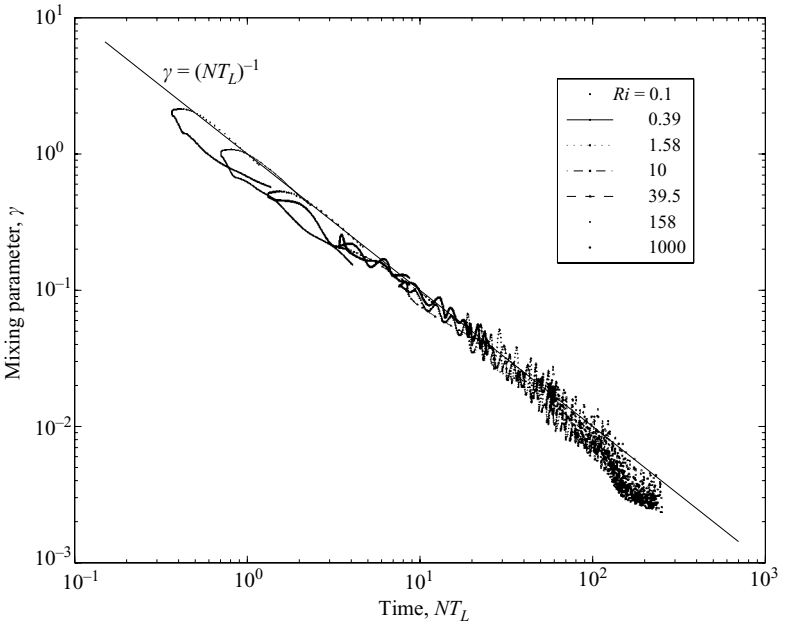

FIGURE 16. The mixing coefficient γ in the PPH model as a function of the local value of NT_L where $T_L = E/\epsilon$ is the Lagrangian time scale. The solid line shows that $\gamma \sim (NT_L)^{-1}$.

As noted by Hunt (1985), multiplying (4.1) by ρ' and ensemble averaging (assuming homogeneity) yields

$$\epsilon_\rho = \kappa\overline{(\nabla\rho' \cdot \nabla\rho')} = \gamma N \overline{\rho'^2}, \tag{4.2}$$

which can be used to estimate γ from the scalar dissipation rate ϵ_ρ. Estimates of γ obtained in this way are shown plotted in figure 16 as a function of the local stability parameter NT_L, where $T_L = E/\epsilon$ is the decay time scale for the total energy E. It can be seen that the mixing coefficient is not constant, but evolves with time and reduces as the stratification strengthens. Values are in the range $0.001 \lesssim \gamma \lesssim 1$. However, plotted in this form, all the data collapse onto a single line $\gamma \simeq (NT_L)^{-1}$, suggesting that N^{-1} is not the appropriate choice of time scale in (4.1), and that a reformulation of the PPH mixing model as

$$\kappa\nabla^2\rho' = -\gamma' {T_L}^{-1}\rho', \tag{4.3}$$

where $\gamma' \sim 1$, provides a good description of the mixing in this transient flow for all times and all stratification strengths. In this modified model the time scale T_L, which is insensitive to stratification (see § 4.1), controls the mixing process rather than N^{-1}. This formulation is consistent with the original model suggested by Csanady (1964). Mixing models of this form are also widely used in PDF methods for application to reacting flows where they are known as 'interaction by exchange with the mean' or IEM models (see e.g. Pope 2000, p. 547).

Values of the mixing coefficient from (4.3), namely $\gamma' = \epsilon_\rho T_L/\overline{\rho'^2}$, are plotted in figure 17 as a function of time and for various Ri numbers. Note that for the initial conditions used in the present simulations, it can be shown that these estimates give $\gamma' \to Pr^{-1}/2$ as $t \to 0$. Although there are significant temporal oscillations in γ' for

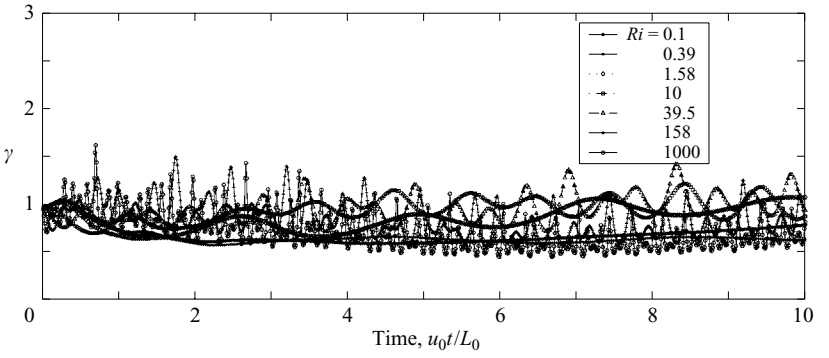

FIGURE 17. The mixing coefficient γ' (calculated from (4.3)) as a function of time u_0t/L_0 for varying Ri.

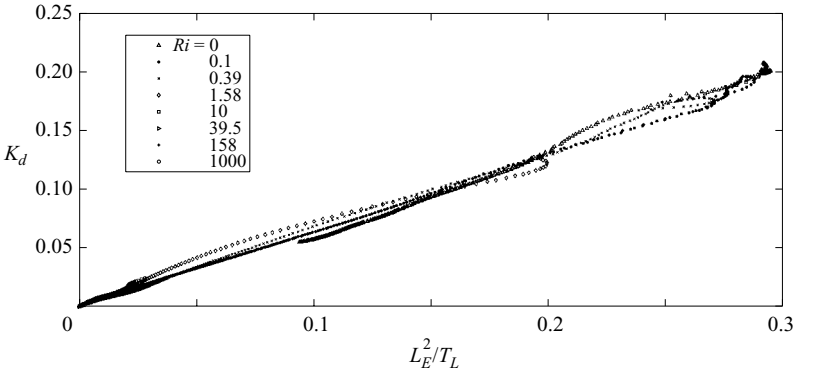

FIGURE 18. The diapycnal turbulent diffusivity plotted as a function of ${L_E}^2/T_L$ for a range of Ri numbers and for times $u_0t/L_0 > 1$.

the strongly stable cases, if these oscillations are averaged out, the mixing coefficient is approximately constant and insensitive to stratification strength. An average value of $\gamma' \simeq 0.7$ may be deduced from this data.

An alternative interpretation of these results is in terms of the mechanical-to-scalar time-scale ratio $\epsilon_\rho T_L/(\overline{\rho'^2}/2) = 2\gamma' \simeq 1.4$. This time-scale ratio is widely used in second moment closure models (see e.g. Pope 2000). It is evident from figures 16 and 17 that despite the wide range of stratification strengths, the time-scale ratio remains similar to values ($\sim$1.5) reported for experiments on thermally stratified decaying grid turbulence (Warhaft 2000). Values obtained from DNS of stationary (forced), isotropic, unstratified turbulence (Yeung 2001) are somewhat higher ($\sim$2) and vary slowly with Reynolds and Prandtl numbers. The insensitivity of the time-scale ratio to stratification has important (simplifying) implications for modelling.

The *IEM* mixing model (equation (4.3)) predicts the diapycnal (turbulent) diffusivity in these flows as (using (2.12))

$$K_d = \frac{\epsilon_\rho}{(\partial\overline{\rho}/\partial z)^2} = \gamma' \frac{{L_E}^2}{T_L}, \tag{4.4}$$

where $L_E = (\overline{\rho'^2})^{1/2}/|\partial\overline{\rho}/\partial z|$ is the Ellison 'overturning' length scale. This prediction is tested in figure 18. The initial transient in the development of the scalar field for

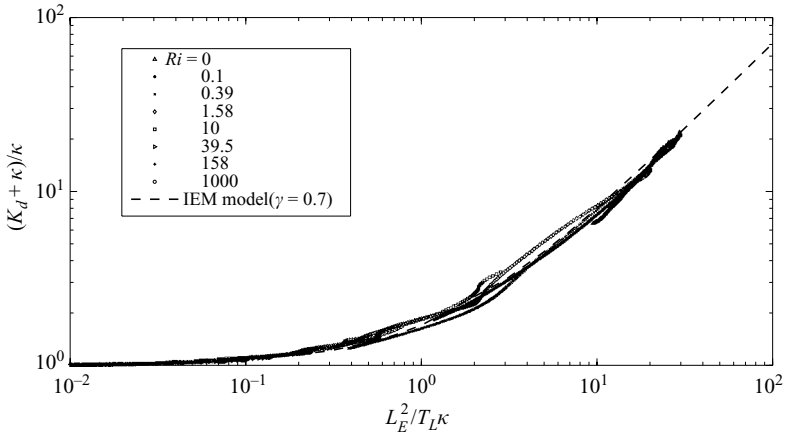

FIGURE 19. The total diapycnal diffusivity, normalized by the molecular diffusivity, plotted as a function of ${L_E}^2/T_L\kappa$ for a range of Ri numbers and for times $u_0t/L_0 > 1$. The dashed line is the *IEM* model prediction (equation (4.5)).

times $u_0t/L_0 < 1$ has been excluded from the plot. It can be seen that K_d increases linearly with ${L_E}^2/T_L$ as required by (4.4), with a slope $\gamma' \simeq 0.7$. To place these results in the context of a general scaling prediction, the total diapycnal diffusivity $K_d + \kappa$ is shown plotted in non-dimensional form in figure 19 for comparison with the *IEM* model prediction, namely

$$(K_d + \kappa)/\kappa = 1 + \gamma' \frac{{L_E}^2}{T_L\kappa} . \tag{4.5}$$

Plotted in this form, the data collapse well and are consistent with the *IEM* model prediction. The parameter $Pe_t = {L_E}^2/T_L\kappa$ may be interpreted as a turbulent Péclet number based on the vertical overturning scale L_E and a velocity scale L_E/T_L. In the most stable cases ($Ri \gtrsim 40$), the values of Pe_t are less than one and the total diapycnal diffusivity reverts to molecular values. When $Pe_t > 1$ the turbulent diffusivity starts to dominate. The prediction of (4.5), supported by the data shown in figure 19, is important because it establishes a direct link between the model for Lagrangian mixing and the diapycnal diffusivity.

It has been suggested (see Fox 1996 and Pope 1998 for a detailed discussion) that small-scale mixing should be independent of the velocity at high Reynolds numbers, i.e. that the correlation $\overline{w\nabla^2\rho'}$ should approach zero in that limit. The *IEM* model is inconsistent with this and predicts (from (4.3))

$$\kappa\overline{w\nabla^2\rho'} = -\epsilon_\rho\overline{w\rho'}/\overline{\rho'^2}. \tag{4.6}$$

An 'interaction by exchange with the conditional mean' model (*IECM*) may be defined as

$$\kappa\nabla^2\rho' = -\gamma_c'{T_L}^{-1}(\rho - \overline{\rho \mid w}) = -\gamma_c'{T_L}^{-1}(\rho' - \overline{\rho' \mid w}), \tag{4.7}$$

where the conditional scalar average $\overline{\rho \mid w}$ (the expected value of ρ given w) is used as the reference density in (4.3). Since $\overline{w\rho'} = \overline{w\overline{\rho' \mid w}}$, it follows that the *IECM* model enforces the constraint $\overline{w\nabla^2\rho'} = 0$.

Computed values of the correlations $\kappa\overline{w\nabla^2\rho'}$ from the simulations are plotted in figure 20 as a function of time and for various Ri numbers. Also shown are

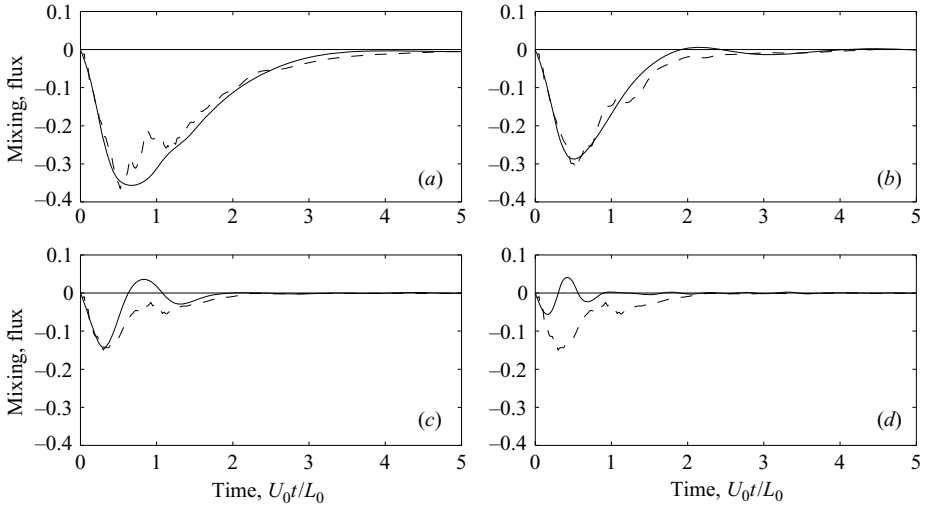

FIGURE 20. Correlations between vertical velocity and mixing as a function of time (dashed lines) for (*a*) $Ri = 0.39$; (*b*) $Ri = 1.58$; (*c*) $Ri = 10.0$; (*d*) $Ri = 39.5$. The solid lines are the *IEM* model predictions (equation (4.6)).

the *IEM* model predictions (equation (4.6)). It can be seen that the correlations are generally non-zero and negative, but their magnitudes decrease for times $t \gtrsim 1$ and with increasing Ri. The *IEM* model predictions are generally consistent with the simulation data, especially for the less stable cases where diapycnal mixing is stronger. The *IEM* model therefore performs better than the *IECM* model at these low Re numbers.

If the conditional average $\overline{\rho' \mid w}$ is assumed to vary approximately linearly with w (Fox 1996; Pope 1998),

$$\overline{\rho' \mid w} = \frac{\overline{w\rho'}}{\overline{w^2}}\, w, \tag{4.8}$$

then it follows from (4.3) and (4.7) that the mixing coefficient γ_c' for the *IECM* model is given by

$$\gamma_c' = \gamma' \left(1 - R_{\rho w}^2\right)^{-1}, \tag{4.9}$$

where $R_{\rho w} = \overline{w\rho'}/(\overline{\rho'^2}\,\overline{w^2})^{1/2}$ is the flux correlation coefficient. In the present simulations, $R_{\rho w} \to 1$ as $t \to 0$, so that (4.9) is unrealistic near $t = 0$. Disregarding the initial transient which is an artefact of the specified initial conditions, the differences between γ' and γ_c', as given by (4.9), are small in the stably stratified cases since the flux correlation coefficient is suppressed by the stratification.

4.4. *Flow structure*

In this section, we present features of the flow structure as it evolves. We focus on over-turning motions and their relationship to mixing.

Visualization of the vertical density gradients can indicate the presence (or absence) of overturns in a stratified flow. Three-dimensional plots of the vertical density gradient fields are shown in figure 21 at times $u_0t/L_0 = 1, 2, 3$ and 4, and for $Ri = 0.39,\ 1.58$ and 10. The isosurface levels shown in the plot mark the boundaries of overturning regions (i.e. where $\partial\rho/\partial z = 0$) while non-overturning regions are transparent. It can be seen that overturns disappear in all cases at times, $Nt \gtrsim 2\pi$,

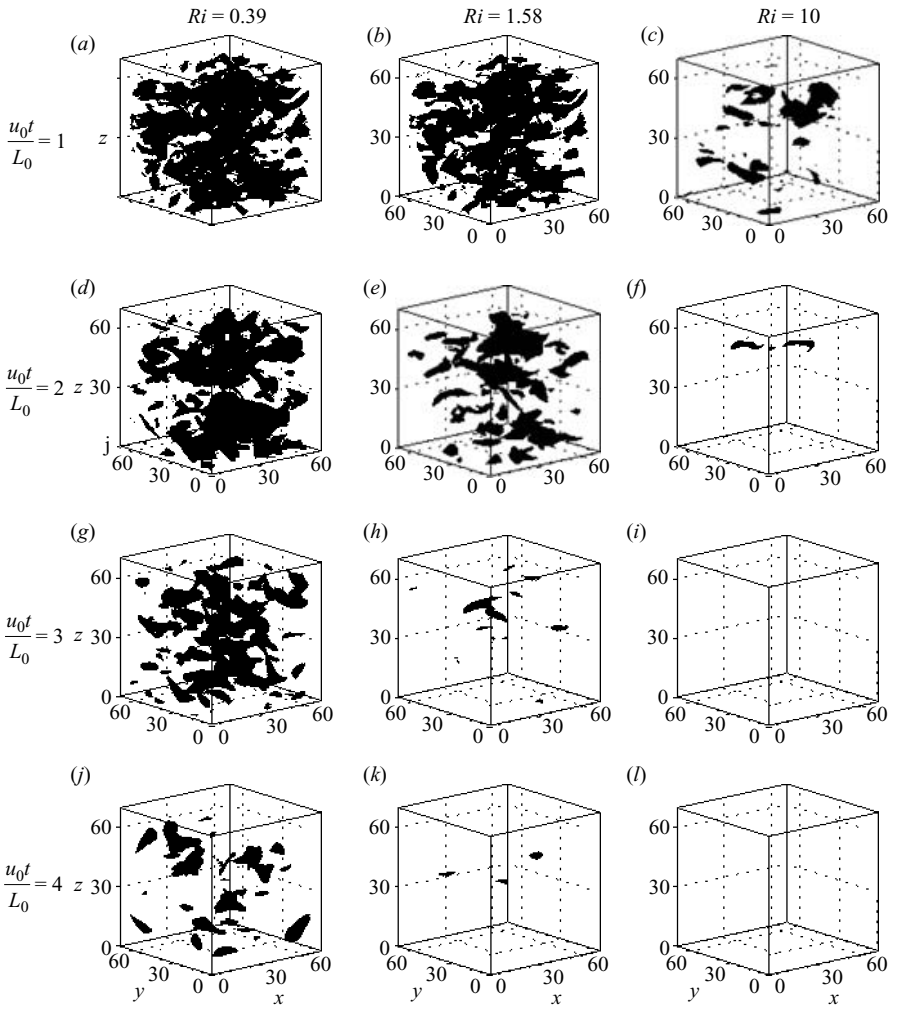

FIGURE 21. Isosurfaces of vertical density gradient for (*a*) $Ri = 0.39$, $Nt = 0.6$; (*b*) $Ri = 1.58$, $Nt = 1.3$; (*c*) $Ri = 10.0$, $Nt = 3.2$; (*d*) $Ri = 0.39$, $Nt = 1.2$; (*e*) $Ri = 1.58$, $Nt = 2.5$; (*f*) $Ri = 10.0$, $Nt = 6.3$; (*g*) $Ri = 0.39$, $Nt = 1.9$; (*h*) $Ri = 1.58$, $Nt = 3.8$; (*i*) $Ri = 10.0$, $Nt = 9.5$; (*j*) $Ri = 0.39$, $Nt = 2.5$; (*k*) $Ri = 1.58$, $Nt = 5.0$; (*l*) $Ri = 10.0$, $Nt = 12.6$. The surface levels are at the limiting value of zero, values greater than zero imply unstable gradients.

i.e. after about one buoyancy period. This is also when the mixing collapses (see figure 11*b*), which shows that mixing is strongly related to the presence of unstable density gradients and hence overturns in the flow.

Visualizations of the density fields by Metais & Herring (1989) revealed similar changes to those described here. They linked this change at $Nt \gtrsim 2\pi$ to the behaviour of the Ellison scale L_E, noting that $L_E \sim L_o \sim L_k$ at these times, where $L_o = (\epsilon/N^3)^{1/2}$ is the Ozmidov scale and $L_k = (\nu^3/\epsilon)^{1/4}$ is the Kolmogorov microscale.

Diamessis & Nomura (2004) have previously shown that overturn peripheries are sites of high diapycnal mixing. We visualized the flow fields associated with some extreme mixing events to identify the structures associated with these events. In figure 22, isosurfaces of the vertical density gradients as well as two-dimensional slices in the (x, z)-, (y, z)- and (x, y)-planes for some high mixing events are shown. It

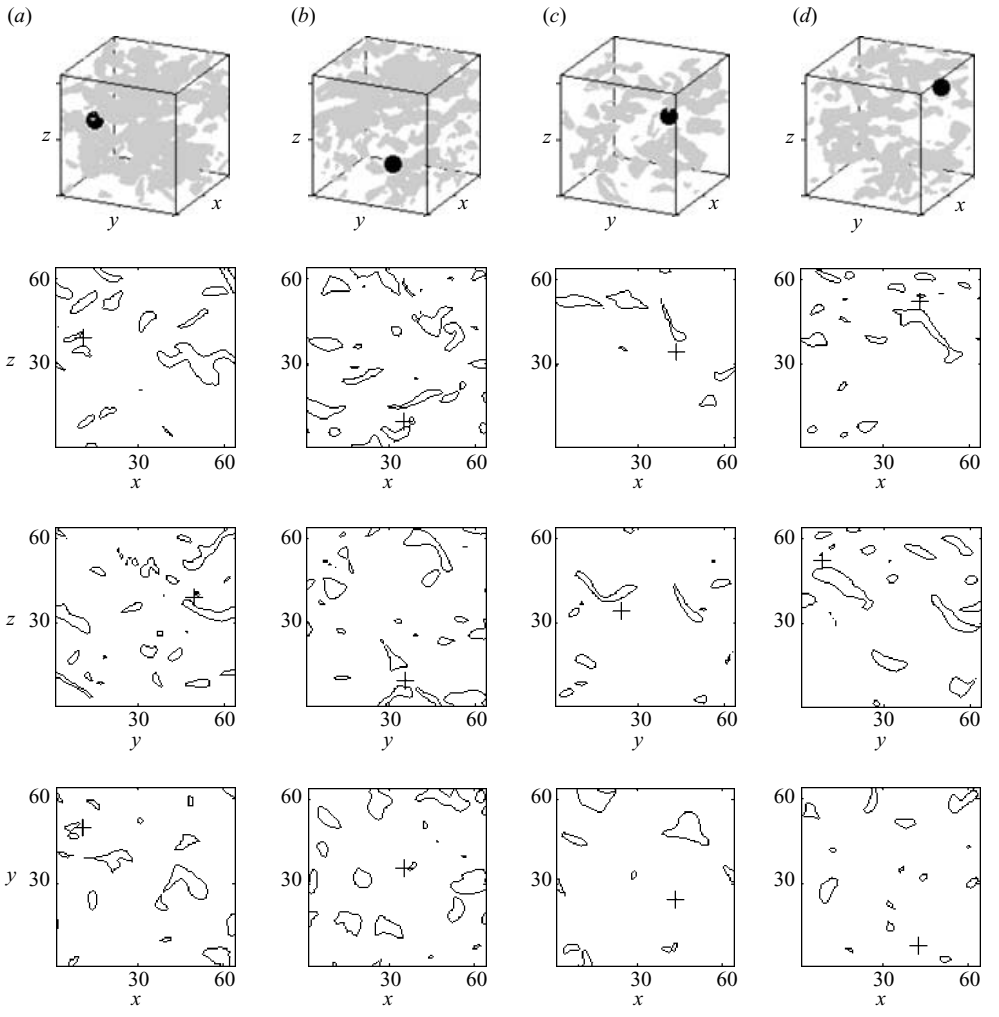

FIGURE 22. Isosurfaces and contour plots of the vertical density gradient in the (x, z)-, (y, z)- and (x, y)-planes for high mixing events for (*a*) $Ri = 0.39$, $u_0 t/L_0 = 0.725$; (*b*) $Ri = 0.39$, $u_0 t/L_0 = 1.100$; (*c*) $Ri = 1.58$, $u_0 t/L_0 = 0.425$; (*d*) $Ri = 1.58$, $u_0 t/L_0 = 1.475$. The crosses and black filled circles indicate the position of the particle at the high mixing event. The contour levels shown mark the critical value of zero beyond which gradients become unstable.

is clearly evident that these intermittent extreme mixing events occurred close to, but not within, overturning regions. A simple conceptual model of an overturning region that is consistent with these observations is depicted schematically in figure 23 (after Ivey *et al.* 2000), and shows how the wrapping and folding of isopycnals can give rise to high scalar gradients (and diapycnal fluxes) around the periphery of overturns.

Isosurfaces of the enstrophy (mean-square vorticity) for $Ri = 0.39$, 1.58, 10 and 158 and at times $u_0 t/L_0 = 1, 2, 3$ and 4 are shown in figure 24 (the surface levels are three times the mean values). For the high Ri cases, there is a clear emergence of randomly distributed 'pancake-shaped' structures with near horizontal orientation (see figure 24*h*, *l*, *p*), as also previously reported by Kimura & Herring (1996). These features start becoming evident for times $Nt \gtrsim 4\pi$ so that it appears that their emergence is related to the suppression of overturns and decoupling of the vertical

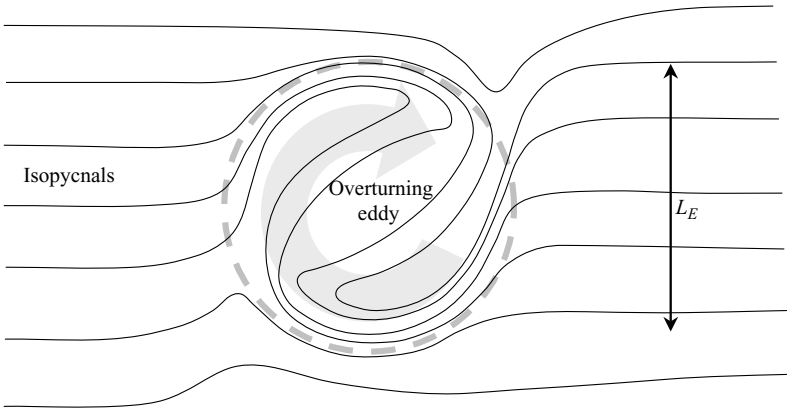

FIGURE 23. Schematic representation of the wrapping and folding of isopycnals by an overturning eddy resulting in high scalar gradients and diapycnal fluxes around the periphery of the overturn (after Ivey *et al.* 2000).

and horizontal dynamics of the flow. The main contribution to the enstrophy in these patches is from the horizontal components of the vorticity field.

To investigate further the flow structure associated with these 'pancake' enstrophy patches, we have plotted the tracks for 8 sets of 64 fluid particles, each set originating on a different (x, y)-plane. The (x, y)-projection of these streaklines for the case $Ri = 1000$ and for times $5 \leqslant u_0 t/L_0 \leqslant 10$ are shown in figure 25. In this strongly stratified case, the particles are essentially constrained to horizontal planes. At these late times, corresponding to $Nt \gtrsim 150$, there is evidence of the emergence of large-scale horizontal vortices in a layered formation with strong vertical variability. For example, circular vortex motion is evident in the streak patterns at $z = 34, 42$ and 50 in figure 25, but the patterns are different at each of these z-levels. Streaklines at other intermediate z-levels do not show any evidence of vortex motion. These features were predicted by Riley *et al.* (1981) on the basis of a scaling analysis for the low-Froude-number regime (see Riley & Lelong 2000 for a more recent review). Praud, Fincham & Sommeria (2005) observed and studied similar features in laboratory experiments that focused on this low-Froude-number regime. The visualization in figure 25 is apparently the first time that direct evidence for the emergence of these modes from initially isotropic simulations of stably stratified turbulence has been reported. Similar structures are also evident in the simulations at $Ri = 158$, but for smaller Ri numbers the streak patterns start becoming more disorganized, suggesting that these modes only become apparent at very large times, say $Nt \gtrsim 50$. The 'pancake' enstrophy patches in figure 24 appear to be associated with shear layers between the layered vortex modes. It has been suggested (e.g. Riley & Lelong 2000; Riley & deBruynKops 2003) that at high Re numbers, these shear layers could become locally unstable, thereby providing an additional source of turbulence and mixing in these flows.

5. Conclusions

In this study, we have exploited the detailed information available from DNS to investigate the properties of Lagrangian mixing in transient (decaying) homogeneous stably stratified turbulence. This is intended as a first step towards developing improved models for dispersion and mixing in stably stratified environmental flows.

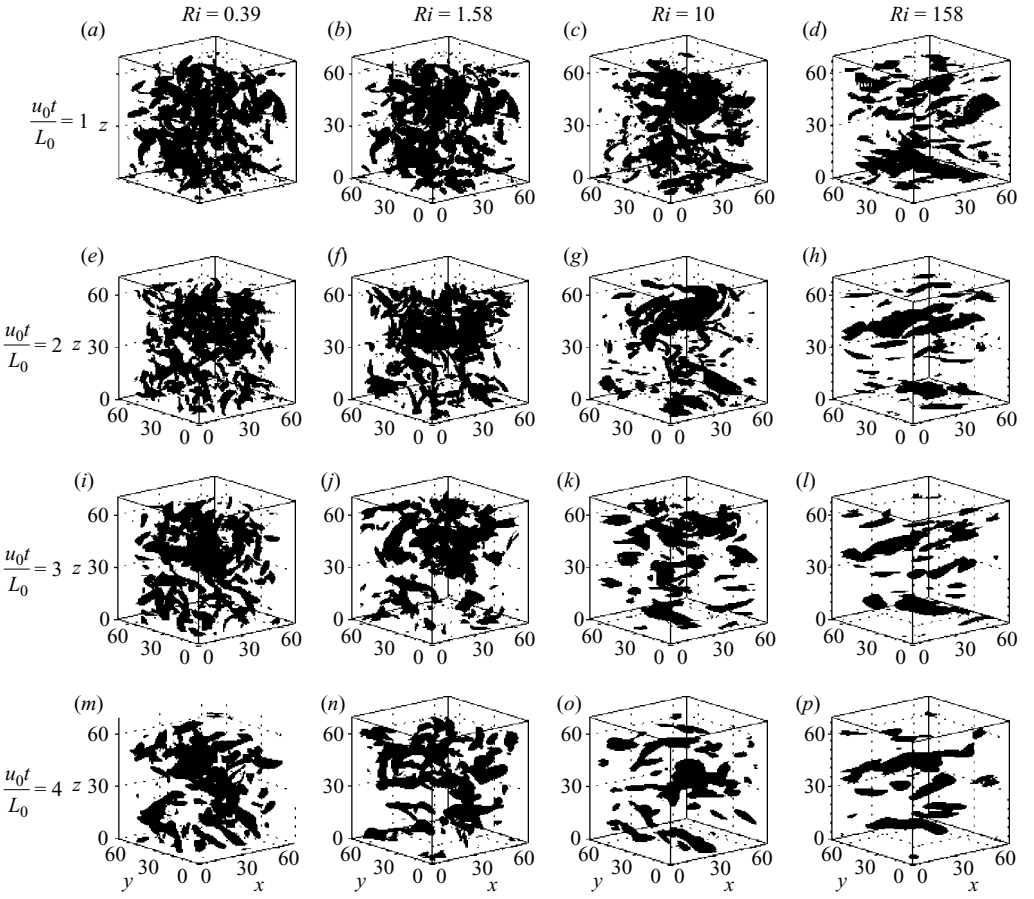

FIGURE 24. Isosurfaces of enstrophy for (*a*) $Ri = 0.39$, $Nt = 0.6$; (*b*) $Ri = 1.58$, $Nt = 1.3$; (*c*) $Ri = 10.0$, $Nt = 3.2$; (*d*) $Ri = 158$, $Nt = 12.6$; (*e*) $Ri = 0.39$, $Nt = 1.2$; (*f*) $Ri = 1.58$, $Nt = 2.5$; (*g*) $Ri = 10.0$, $Nt = 6.3$; (*h*) $Ri = 158$, $Nt = 25.1$; (*i*) $Ri = 0.39$, $Nt = 1.9$; (*j*) $Ri = 1.58$, $Nt = 3.8$; (*k*) $Ri = 10.0$, $Nt = 9.5$; (*l*) $Ri = 158$, $Nt = 37.7$; (*m*) $Ri = 0.39$, $Nt = 2.5$; (*n*) $Ri = 1.58$, $Nt = 5.0$; (*o*) $Ri = 10.0$, $Nt = 12.6$; (*p*) $Ri = 158$, $Nt = 50.3$. The surface levels are three times the mean enstrophy values for each case.

A Lagrangian perspective of the mixing following fluid particles has yielded some new insights into the mixing processes in these flows and into the way that the stratification affects them.

The main conclusions concerning the questions outlined in § 1 may be summarized as follows.

(i) The results indicate that small-scale mixing processes dominate the changes in density perturbations ρ' following fluid particles for weak stratification. As the effects of stratification become more significant (at larger Ri and/or for times $Nt \gtrsim 2\pi$), mixing is strongly suppressed and advection within the background mean density gradient starts to dominate the changes in ρ'.

(ii) After a short initial transient, diapycnal displacements due to small-scale mixing dominate the dispersion of fluid particles in all cases, including for weak stratification. The relationship between the diapycnal diffusivity and the vertical dispersion coefficients depends on the stratification. In general, the overall dispersion

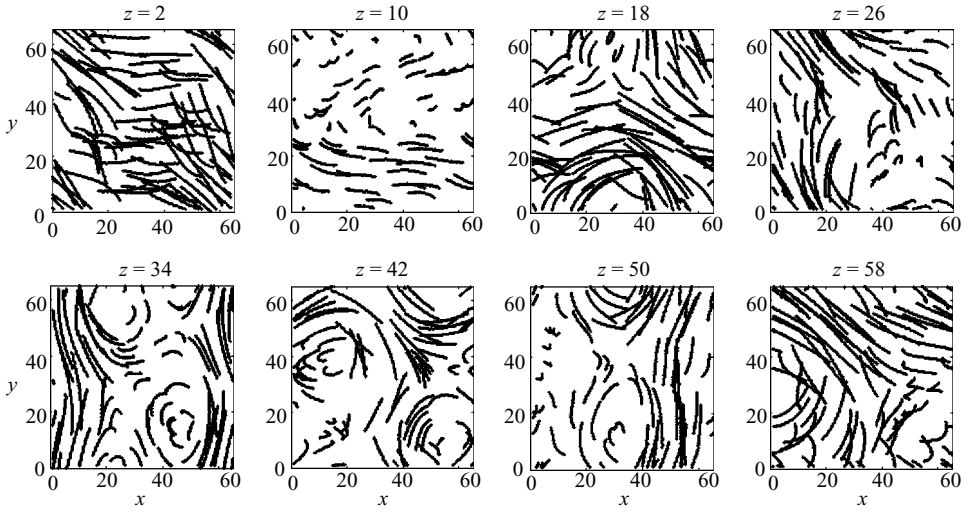

FIGURE 25. Streaklines for $Ri = 1000$ and times $5 < u_0 t/L_0 < 10$. Each panel contains streaklines for 64 particles released on a specific horizontal plane as indicated by the z-grid coordinate above each one.

coefficient K_z is a poor indication of the diapycnal diffusivity. This is mainly because significant reversible (or adiabatic) contributions to the flux can occur in these flows, in particular as Ri increases. The irreversible diapycnal mixing appears to remain largely unaffected by internal wave motions. However, this mixing is strongly suppressed by the stratification because buoyancy forces limit the vertical displacements of fluid particles and ultimately suppress the overturning motions that are required to generate diapycnal mixing.

(iii) The time scale for the density changes following fluid particles has been found to be approximately independent of the stratification for these transient flows. In particular, it does not scale on N^{-1} as suggested by the PPH model. Instead, the mixing time scale is linked to the energy decay time scale T_L which is relatively insensitive to the stratification. We have shown how the mixing model predicts a parameterization for the diapycnal diffusivity in these flows, e.g. the *IEM* model predicts that the diapycnal diffusivity scales on the Ellison overturning length scale and energy decay time scale.

(iv) There are large changes in the structure of these transient flows as they evolve under the influence of buoyancy forces. Two features of these changes are important with respect to mixing. First is an approximate decoupling of the vertical and horizontal motions with the former becoming dominated by internal waves and the latter comprising quasi-horizontal modes (but with large vertical variability). The second is the suppression of overturning motions. The Lagrangian mixing rates have been found to be strongly linked to changes in the flow structure as it evolves. In particular, mixing is closely associated with overturning events. However, there is evidence that the strongest mixing does not occur within these overturning regions, but around their periphery.

The results reported here have important implications for the development of improved models for diffusion in stably stratified turbulence. In particular, our results confirm the basic notion, highlighted by PPH, that such models should properly account for the role of small scale mixing processes in changing the densities of

fluid particles. This issue is also important for the modelling of turbulent reactive flows and some of the developments in that field could perhaps be applied to stably stratified flows. The work of Das & Durbin (2005) essentially does this. However, their Lagrangian stochastic model is statistically linked to existing second moment closure models and does not seem to provide specific new insights into details of the mixing process. Their mixing model is similar to the *IEM* model, but includes an additional stochastic diffusion term. The *IEM* model is deterministic, and although it gives good results in terms of statistical averages, it does not account for the detailed temporal features of the mixing that are described in § 4.3.1, e.g. intermittency. The implications of this remain to be clarified by future work.

Application of the results reported here to real geophysical flows is limited by the low Reynolds number of the simulations and the absence of other common features of naturally occurring flows, such as shear. Therefore, two useful extensions of the present work would be as follows.

(a) To study Lagrangian mixing in flows that include the effects of shear in addition to stable stratification. Hunt (1985) indicates that there is evidence that the mixing between fluid particles increases with shear. In the context of the mixing model, this suggests a possible increase in the mixing coefficient γ' due to shear.

(b) To expand the Reynolds and Prandtl (or Schmidt) number range of the simulations to clarify their influence on mixing processes in stably stratified flows. For example, at higher Reynolds numbers, the local instabilities observed by Riley & deBruynKops (2003) could lead to additional overturns and mixing at late times.

The authors thank the referees for their comments and recommendations and in particular acknowledge the referee who suggested the conditional model in § 4.3.3. We thank Jim Riley for providing his DNS code for this work. D.D.S. is grateful to Jim Rottman for his support and many stimulating discussions on aspects of this work during visits to UCSD. He also acknowledges Julian Hunt, whose ideas originally inspired this work. We thank Bob Street and Jim Rottman for their comments on a draft of the paper.

REFERENCES

Britter, R. E., Hunt, J. C. R., Marsh, G. L. & Synder, W. H. 1983 The effects of stratification on turbulent diffusion and the decay of grid turbulence. *J. Fluid Mech.* **127**, 27–44.

Csanady, G. T. 1964 Turbulent diffusion in a stratified flow. *J. Atmos. Sci.* **21**, 439–447.

Das, S. K. & Durbin, P. A. 2005 A Lagrangian stochastic model for dispersion in stratified turbulence. *Phys. Fluids* **17**, 1–10.

Diamessis, P. J. & Nomura, K. K. 2004 The structure and dynamics of overturns in stably stratified homogeneous turbulence. *J. Fluid Mech.* **499**, 197–229.

Fox, R. O. 1996 On velocity-conditioned scalar mixing in homogeneous turbulence. *Phys. Fluids* **8**, 2678–2691.

Gregg, M. C. 1987 Diapycnal mixing in the thermocline. *J. Geophys. Res.* **92**, 5249–5286.

Hanazaki, H. & Hunt, J. C. R. 1996 Linear processes in unsteady stably stratifed turbulence. *J. Fluid Mech.* **318**, 303–337.

Hunt, J. C. R. 1982 Diffusion in the stable boundary layer. In *Atmospheric Turbulence and Air Pollution Modelling* (ed. F. T. M. Nieuwstadt & H. van Dop), pp. 231–274. Reidel.

Hunt, J. C. R. 1985 Diffusion in the stably stratified atmospheric boundary layer. *J. Climate Appl. Met.* **24**, 1187–1195.

Hunt, J. C. R., Stretch, D. D. & Britter, R. E. 1988 Length scales in stably stratified turbulent flows and their use in turbulence models. In *Stably Stratified Flow and Dense Gas Dispersion* (ed. J. S. Puttock), pp. 285–322. Clarendon.

Ivey, G. N., Winters, K. B. & De Silva, I. P. D. 2000 Turbulent mixing in a sloping benthic boundary layer energized by internal waves. *J. Fluid Mech.* **418**, 59–76.

Kaneda, Y. & Ishida, T. 2000 Suppression of vertical diffusion in strongly stratified turbulence. *J. Fluid Mech.* **402**, 311–327.

Kimura, Y. & Herring, J. R. 1996 Diffusion in stably stratified turbulence. *J. Fluid Mech.* **328**, 253–269.

Linden, P. F. 1979 Mixing in stratified fluids. *Geophys. Astrophys. Fluid Dyn.* **13**, 3–23.

Metais, O. & Herring, J. R. 1989 Numerical simulations of freely evolving turbulence in stably stratified fluid. *J. Fluid Mech.* **202**, 117–148.

Nappo, C. J. & Johansson, P.-E. 1999 Summary of the Lövånger international workshop on turbulence and diffusion in the stable planetary boundary layer. *Boundary-Layer Met.* **90**, 345–374.

Pearson, H. J., Puttock, J. S. & Hunt, J. C. R. 1983 A statistical model of fluid-element motions and vertical diffusion in a homogeneous stratified turbulent flow. *J. Fluid Mech.* **129**, 219–249.

Pope, S. B. 1994 Lagrangian PDF methods for turbulent flows. *Annu. Rev. Fluid Mech.* **26**, 23–63.

Pope, S. B. 1998 The vanishing effects of molecular diffusivity on turbulent dispersion: implications for turbulent mixing and the scalar flux. *J. Fluid Mech.* **359**, 299–312.

Pope, S. 2000 *Turbulent Flows*. Cambridge University Press.

Praud, O., Fincham, A. M. & Sommeria, J. 2005 Decaying grid turbulence in a strongly stratified fluid. *J. Fluid. Mech.* **522**, 1–33.

Riley, J. J. & deBruynKops, S. M. 2003 Dynamics of turbulence strongly influenced by buoyancy. *Phys. Fluids* **15**, 2047–2059.

Riley, J. J. & Lelong, M. P. 2000 Fluid motions in the presence of strong stable stratification. *Annu. Rev. Fluid Mech.* **32**, 613–657.

Riley, J. J., Metcalfe, R. W. & Weissman, M. A. 1981 Direct numerical simulations of homogeneous turbulence in density stratified fluids. In *Nonlinear Properties of Internal Waves AIP Conf. Proc.* 76 (ed. B. J. West), pp. 79–112. AIP.

Shih, L. H., Koseff, J. R., Ivey, G. N. & Ferziger, J. H. 2005 Parameterization of turbulent fluxes and scales using homogeneous sheared stably stratified turbulence simulations *J. Fluid. Mech.* **525**, 193–214.

Stretch, D. D., Rottman, J. W., Venayagamoorthy, S. K. & Nomura, K. K. 2001 Transient mixing events in stably stratified turbulence. *14th Australasian Fluid Mechanics Conference, Adelaide, Australia, December 10–14, 2001*.

Taylor, G. I. 1921 Diffusion by continuous movements. *Proc. Lond. Math. Soc. Ser. 2* **20**, 196–212.

Townsend, A. A. 1976 *The Structure of Turbulent Shear Flow*. Cambridge University Press.

Venkatram, A., Strimaitis, D. & Dicristofaro, D. 1984 A semiempirical model to estimate vertical dispersion of elevated releases in the stable boundary layer. *Atmos. Environ.* **18**, 923–928.

Warhaft, Z. 2000 Passive scalars in turbulent flows. *Annu. Rev. Fluid Mech.* **32**, 203–240.

Winters, K. B. & D'Asaro, E. A. 1996 Diascalar flux and the rate of fluid mixing. *J. Fluid Mech.* **317**, 179–193.

Winters, K. B., Lombard, P. N., Riley, J. J & D'Asaro, E. A. 1995 Available potential energy and mixing in density-stratified fluids. *J. Fluid Mech.* **289**, 115–128.

Yeung, P. K. 2001 Lagrangian characterisitics of turbulence and scalar transport in direct numerical simulations. *J. Fluid Mech.* **427**, 241–274.

Yeung, P. K. 2002 Lagrangian investigations of turbulence. *Annu. Rev. Fluid Mech.* **34**, 115–142.

Yeung, P. K. & Pope, S. B. 1988 An algorithm for tracking fluid particles in numerical simulations of homogeneous turbulence. *J. Comput. Phys.* **79**, 373–416.